MULTIPHASE FLOW METERING USING A PRESSURE DROP BASED METERING DEVICE

by

Chaitanya Nagabathula

Submitted in partial fulfilment of the requirements
for the degree of Master of Applied Science

at

Dalhousie University
Halifax, Nova Scotia
April 2018

For my family

TABLE OF CONTENTS

List of Tables

List of Figures

Abstract

A dual-pressure drop based flow measurement device (DPDE) was developed taking advantage of the compressibility of two-phase flow. By creating a pressure drop between two crimped pipe elements with restrictions, a variation in density and volumetric flow rate was created. This variation caused by flow expansion is used to predict mass flow rate and gas fraction of two-phase flow. An air-water-ethanol mixture was used, and the device was tested for gas fractions ranging from 0-85% with mass flow rates varying from 30-100 kg/h. The predicted mass flow rate and density are compared to results obtained from a Coriolis meter and gas/liquid feed rates to the system. Average errors of ±5 kg/h and ±100 kg/m^3 were observed for mass flow rate and density, respectively.

List of Abbreviations and Symbols Used

A	Area of cross-section (m^2)
C_d	Coefficient of discharge (dimensionless)
D	Pipe diameter (m)
F_a	Thermal expansion correction factor (dimensionless)
Fr	Froude number (dimensionless)
g	Gravitational constant (9.807 m/s^2)
I_o	Initial intensity (photon/m^2-s)
I_d	Resultant intensity (photon/m^2-s)
K_L	Two-phase correction factor (dimensionless)
$\dot{m}$	Mass flow rate (kg/h)
$\dot{m}'$	Apparent mass flow rate (kg/h)
P	Absolute pressure (Pa)
P_{avg}	Average pressure (Pa)
S	Slip ratio (dimensionless)
T	Temperature (ºC)
U_{SG}	Superficial gas velocity (m/s)
x	Mass flow quality (dimensionless)
X	Modified Lockhart-Martinelli parameter (dimensionless)
Y	Compressibility coefficient (dimensionless)

Symbols

α	Gas fraction (dimensionless)
β	Orifice (or throat)-to-pipe diameter ratio (dimensionless)
ρ	Density (kg/m^3)
μ	Viscosity (kg/m·s)
ΔP	Differential pressure (Pa)

Subscripts

atm	Atmospheric conditions
D	Downstream section
G	Gas
L	Liquid
o	Orifice
SP	Single-phase flow
TP	Two-phase flow
U	Upstream section
v	Venturi

Abbreviations

ANN	Artificial neural networks
BF	Blockage factor
CFD	Computational fluid dynamics
DPDE	Dual-pressure drop element device
EBR	Ebullated bed reactor
LPM	Liters per minute
MCNP	Monte Carlo N-particle
MPFM	Multiphase flow metering
OR	Over-reading
RMS	Root-mean-square
RPM	Revolutions per minute
RSD	Relative standard deviation

Acknowledgements

I would like to express my sincere gratitude to my supervisor Dr. Adam Donaldson for his patience, motivation and immense knowledge. I am deeply appreciative of his commitments of time, ideas, and financing during my degree. His broad knowledge and experience contributed significantly to this research work and in writing this thesis. It was a delightful experience to work under his supervision and mentorship.

I would also like to thank Dr. Jan Haelssig and Dr. Jean F. Bousquet for their insightful comments and encouragement. Their valuable feedback helped a lot in enhancing the quality of this work.

Finally, I would like to thank my friends and family for their unfailing support and continuous encouragement throughout this endeavour.

Chapter 1 INTRODUCTION

The focus on multiphase flow began in the 1960s with researchers attempting to model two-phase flow by exploring boiling and condensation (Chisholm, 1967; Hewitt, 2013; Hewitt and Wallis, 1963; Wallis, 1962). Their efforts intensified during the 1970s and 1980s to investigate different flow patterns in multiphase flow and by examining the effects of different diameters, operating pressures, flow rates and orientations (Barnea, 1987; Barnea et al., 1982; Taitel et al., 1980). Experimental work done since then was predominantly focused on applications for the petroleum industry and for nuclear plants (Meribout et al., 2010; Wylie et al., 2006).

Multiphase flow is generally defined as a stream consisting of two or more phases flowing simultaneously in a system. Multiphase flow metering (MPFM) is defined as the individual measurement of phases in the multiphase flow. MPFM has potential applications in the layout of production facilities, well testing, reservoir management, production allocation, production monitoring, capital and operating expenses and fiscal metering or custody transfer (Falcone et al., 2009; Falcone et al., 2002).

Traditionally, MPFM is done by separating the heterogeneous multiphase mixture into its individual phases, measuring them separately using single phase flow meters before returning them to the multiphase flow line (Wang, 2012). Coriolis meters or turbine flow meters are usually used to measure the liquid flow while vortex flow meters and ultrasonic flow meters are used to measure the gas flow. A challenge of this method of separating and metering the phases is that it is quite expensive and inefficient. To avoid this, in-line MPFMs are preferred over conventional test separators. Continuous metering is possible using MPFMs along with the elimination of test separators, pipelines, manifolds and valve systems. However, MPFMs are sensitive to the physical properties of the phases being measured and may not remain stable over time. Careful operation of the meters is needed to operate them according to the required specifications (Corneliussen et al., 2005).

When applied in a multiphase application, measurements from single-phase flow meters are dependent on the mass flow rate as well as the phase holdup. As gas holdup increases, measurement errors tend to increase as well. A single-phase flow meter cannot typically be used to measure the flowrate and the phase holdup simultaneously, necessitating a coupling of metering devices. This coupled approach works well within the operating range of the instrument but may be subject to a narrow operating range beyond which errors would increase. (Beg and Toral, 1993; Wang, 2012; Xu et al., 2003).

In the recent decades, pressure drop based metering devices have played an important role in the study of multiphase flow metering. Efforts in this area are focused on using a mass flow meter coupled with a density/gas fraction measurement. Dual-pressure drop systems have been used previously (such as a venturi/venturi), but the mass flow rate metering performance is dependent on the entering flow rate and the flow pattern. (Oliveira et al., 2009; Steven, 2002; Zeghloul et al., 2017). By eliminating the flow pattern effects using a homogenizing flow regime and by creating a flow expansion between the pressure drop systems, it is possible to correlate mass flow rates with pressure drops.

The main objective of this thesis is to develop a pressure drop based metering device that can be used to accurately monitor flow rate and phase holdup of an effervescent foaming mixture of air, water and ethanol. Chapter 2 gives a review of various technologies currently available for MPFM including a detailed literature review of pressure drop based metering devices and the correlations commonly used. Chapter 3 describes the motivation for the work, design of the apparatus and the equipment used to conduct the experiments. Chapter 4 discusses the methodology used to develop the correlations and summarizes the results, and Chapter 5 presents the conclusions.

Chapter 2 LITERATURE REVIEW

Commercial in-line multiphase flow meters use technologies like nuclear magnetic resonance spectroscopy, neutron interrogation, gamma ray technologies, electromagnetic measurement methods and the traditional separators for MPFM (G.H. Roshani, 2015). For small-scale applications, orifice meters, V-cone and Venturi meters can be used. They work well for homogeneous flow however, they are not particularly suitable for heterogeneous flow. Instead, it is quite a common practice to use a combination of meters to achieve the desired accuracy (Hong-jian et al., 2005; Oliveira et al., 2009). There are numerous instruments available for MPFM, each involving a different principle and a different metering strategy. The metering strategy is typically based on whether the multiphase flow is separated into individual phases or not. However, the available instruments can be classified into various types based on the parameter they measure.

The parameters that are usually measured and the corresponding instruments used are given in Table 2-1 (Bertani et al., 2010). Detailed description, working principle and the governing equations for each instrument can be found in books on MPFM (Baker, 2005; Falcone et al., 2009).

Table 2-1 *Instruments used to measure parameters of two-phase flow (Bertani et al., 2010)*

Measured parameter	Instruments used
Density	Gamma-ray densitometer
	Neutron interrogation
	Weighing of tube
	Hot film anemometer
	Capacitance/conductance probes
	Ultrasonic flowmeter
Velocity	Pulsed-neutron activation
	Electromagnetic flow meter
	Turbine flowmeter
	Gamma-ray cross correlation
	Neutron cross correlation
	Acoustic cross correlation
	Capacitance/conductivity cross correlation
	Laser Doppler velocimeter
Mass flow	True mass flow meter
	Vibrating tube
	Differential pressure flowmeters
Momentum	Venturi flow meter
	Drag disk

Some of the technologies used to determine the phase fraction are discussed in detail in the following sections. Even though there are many elements available for in-line phase metering, this thesis is primarily focused on developing a pressure drop based metering device.

2.1 Pressure drop based metering devices

Pressure drop based metering devices are inexpensive, easy to manufacture and contain no moving parts. They can be used in any orientation and for most pairs of gases and liquids. However, the output signal from these devices is not linear with the fluid flow. The nature of the flow and the pipe layout may affect the accuracy of the measurement. While these devices generally have good standards, they are susceptible to ageing effects like erosion of sharp edges and the build-up of deposits (Reader-Harris, 2016). Recognizing the advantages and disadvantages of using differential pressure devices for multiphase flow, the ease with which a differential pressure device can be developed cannot be ignored. Hence, the goal of this project was to develop an inexpensive metering device for multiphase flow without compromising the accuracy of the measurement.

2.1.1 Orifice plates

The orifice meter consists of a circular plate with a hole machined through it. The pressure drop across the orifice plate is measured using two pressure taps placed on the upstream and downstream sections of the orifice plate. The differential pressure across the orifice plate is used to determine the mass flow rate of the fluid passing through it. Because of its simple construction and easy installation, orifice meters are often used in industries to measure the flow rate, particularly in small-size lines (De Nevers, 2011; Reader-Harris, 2016).

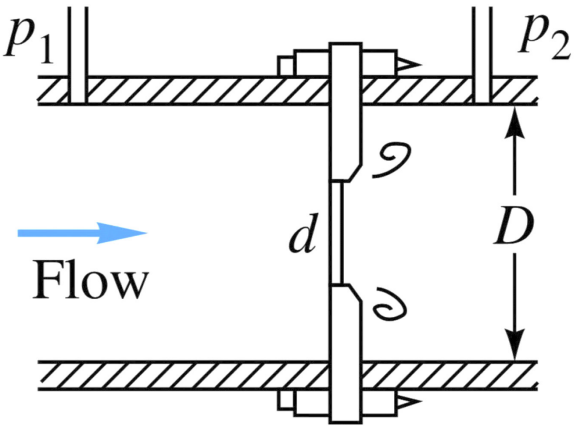

Figure 2-1 *Orifice meter (White, 2003)*

2.1.1.1 Single-phase flow through an orifice

For single-phase flow, the mass flow rate of the fluid $(\dot{m}_L)$ can be correlated to the pressure drop (ΔP) across a differential pressure device by introducing a theoretical coefficient of discharge (C_d) (Oliveira et al., 2009).

$$\dot{m}_L = \left[\frac{C_d A_o Y F_a}{\sqrt{1-\beta_o^4}} \right] \sqrt{2\rho_L \Delta P} \tag{2.1}$$

where A_o is the area of orifice, Y is the compressibility coefficient, β_o is the ratio of orifice diameter to pipe diameter, F_a is the thermal expansion correction factor, and ρ_L is the density of liquid.

For single-phase flow, the fluid is considered to be incompressible making $Y = 1$. Also, if the thermal effects within the fluid are negligible, the thermal expansion correction factor can be taken as 1.

2.1.1.2 Two-phase flow through an orifice

A broad range of empirical models have been developed for orifice plates that correlate the mass flow rate of two-phase flow with pressure drop for different types of flow and fluid combinations. However, in this work only the relevant models namely, Homogeneous model, Chisholm model and Zhang model are discussed in detail.

2.1.1.2.1 Homogeneous model

Homogeneous model for multiphase flow treats the two-phase flow as a pseudo-fluid and provides correction factors to make it applicable for multiphase flow. Hong-jian et al. (2005) modified Eq. 2.1 for multiphase flow calculations by introducing a two-phase correction factor (K_L), which is a function of the mass flow quality or void fraction and the densities of the fluids.

$$\dot{m}_{TP} = \left[\frac{C_{d,TP} A_o Y_{TP} F_a}{\sqrt{1-\beta_o^4}} \right] K_L \sqrt{2\rho_L \Delta P_{TP}} \tag{2.2}$$

Rearranging Eq. 2.2, K_L can be isolated as given by Eq. 2.3.

$$K_L = \frac{\dot{m}_{TP}}{\left[\frac{C_{d,TP} A_o Y_{TP} F_a}{\sqrt{1-\beta_o^4}} \right] \sqrt{2\rho_L \Delta P_{TP}}} \tag{2.3}$$

In developing the correlations for two-phase correction factor, mass flow quality is also used instead of void fraction. The mass flow quality (x) of gas is defined as the ratio of the mass flux of gas to the mass flux of total fluid flow.

$$x = \frac{\dot{m}_G}{\dot{m}_G + \dot{m}_L} \tag{2.4}$$

2.1.1.2.2 Chisholm model

Taking into account the slip between the fluids, a correlation was developed by Chisholm (1977) for an incompressible two-phase flow through orifice plates. The Modified Lockhart-Martinelli parameter (X) was used as a measure to determine the slip ratio (S).

$$S = \left(1 + x\left(\frac{\rho_L}{\rho_G} - 1\right)\right)^{\frac{1}{2}} \qquad For\ X \geq 1 \tag{2.5}$$

$$S = \left(\frac{\rho_L}{\rho_G}\right)^{\frac{1}{4}} \qquad For\ X < 1 \tag{2.6}$$

The original definition of Lockhart-Martinelli parameter is the ratio of friction pressure drops and the Modified Lockhart-Martinelli parameter is defined as the square root of liquid and pressure drop ratio due to acceleration.

$$X = \sqrt{\frac{\Delta P_L}{\Delta P_G}} = \left(\frac{1-x}{x}\right)\sqrt{\frac{\rho_G}{\rho_L}} \tag{2.7}$$

Using the slip-ratio, mass flow quality and the ratio of densities of fluids Chisholm proposed a correlation to estimate the two-phase flow correction factor.

$$K_L = \left(\frac{1}{1-x}\right)\left[1 + \left(\frac{\frac{1}{S}\sqrt{\frac{\rho_L}{\rho_G}} + S\sqrt{\frac{\rho_G}{\rho_L}}}{\left(\frac{1-x}{x}\right)\frac{\sqrt{\rho_G}}{\sqrt{\rho_L}}}\right) + \left(\frac{1}{\left(\frac{1-x}{x}\right)^2\frac{\rho_G}{\rho_L}}\right)\right]^{-\frac{1}{2}} \tag{2.8}$$

2.1.1.2.3 Zhang model for orifice plates

Zhang et al. (1992) proposed a correlation for K_L, using orifice plates and an air-water flow with a mass flow quality less than 1%.

$$K_L = \left\{ \left[x^{\left(1.25+0.25x^{1/3}\right)} \right] \left(\frac{\rho_L}{\rho_G} - 1 \right) + 1 \right\}^{-\frac{1}{2}} \tag{2.9}$$

Some other models available for two-phase flow developed using orifice plates are listed in Table 2-2.

Table 2-2 *Correlations using orifices for two-phase flow (Zeghloul et al., 2017)*

Simpson et al. (1983)	$K_L = \left(\left[1+x\left(S-1\right)\right]\left[1+x\left(S^5-1\right)\right]\right)^{-\frac{1}{2}}; \qquad S = \left(\frac{\rho_L}{\rho_G}\right)^{\frac{1}{6}}$	(2.10)
Morris (1985)	$K_L = \left[x\frac{\rho_L}{\rho_G} + S\left(1-x\right)\right]\left[x + \left(\frac{1-x}{S}\right)\left(1+\frac{\left(S-1\right)^2}{\left(\rho_L/\rho_G\right)^{0.5}-1}\right)\right]$ $S = \begin{cases} \left(1+x\left(\frac{\rho_L}{\rho_G}-1\right)\right)^{0.5} & if\ X>1 \\ \left(\frac{\rho_L}{\rho_G}\right)^{0.25} & if\ X\le 1 \end{cases}; \quad X = \frac{\left(1-x\right)}{x}\left(\frac{\rho_L}{\rho_G}\right)^{0.25}$	(2.11)
Watson et al. (1967)	$K_L = \left(\left(1-x\right)^2\left[1+4.25Y+Y^2\right]\right)^{-\frac{1}{2}}; \quad Y = \left(\frac{x}{1-x}\right)\left(\frac{\rho_L}{\rho_G}\right)^{\frac{1}{2}}$	(2.12)
Collins and Gacesa (1971)	$K_L = \left(\left(1-x\right)^2\left[0.928+0.375\sqrt{Y}+0.913Y\right]^2\right)^{-\frac{1}{2}}; \ Y = \left(\frac{x}{1+x}\right)\left(\frac{\rho_L}{\rho_G}\right)^{\frac{1}{2}}$	(2.13)
James (1965)	$K_L = \left(\left[\left(\frac{\rho_L}{\rho_G}\right)-1\right]x^{1.5}+1\right)^{-\frac{1}{2}}$	(2.14)
Saadawi et al. (1999)	$K_L = \left(1+184x-7293x^2\right)^{-\frac{1}{2}}$	(2.15)

Roul and Dash (2012) investigated the effects of orifice geometry on the pressure drops of two-phase flow by using two pipes with inner diameters of 40 and 60 mm and eight different orifice plates. They used the Eulerian-Eulerian CFD model to determine the pressure drop across the orifices. They also found that, the Morris equation gave better

estimates for the two-phase multiplier for thin orifices while Chisholm model worked better for thicker orifices.

Zeghloul et al. (2017) measured the pressure drop for single and two-phase flow for six different orifices in a vertical upward flow. The average phase fraction for the two-phase flow was determine using a conductance probe. The data obtained from their experiments was used to evaluate the existing models for two-phase flow pressure drop. They found that for vertical flow, Morris and Simpson models gave the most reliable estimates for pressure drop and recommend that they be used for design and metering purposes.

2.1.2 Venturi nozzles

A Venturi meter is comprised of a truncated cone with decreasing cross-sectional area, followed by a throat section and another truncated cone with increasing area of cross-section. The pressure taps are located at the throat and at the upstream section of throat. The difference in the pressure between these locations is used to determine the flow rate of the fluid (De Nevers, 2011). Compared to an orifice plate, the pressure drop generated by a Venturi is less and it also requires less pipe upstream to the meter.

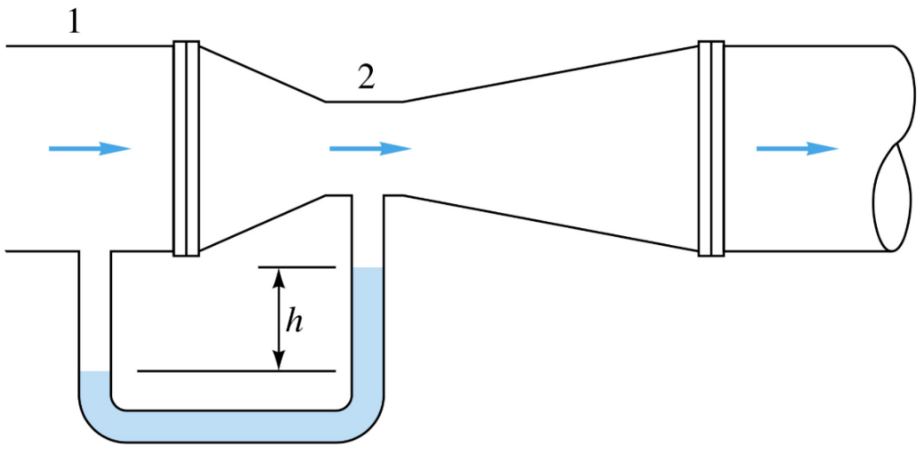

Figure 2-2 *Venturi meter (White, 2003)*

2.1.2.1 Single-phase flow through a Venturi

The mass flow rate equation developed for an orifice (Eq. 2.1) can also be used to determine the mass flow rate of fluid through a Venturi. The area of orifice $\left(A_o\right)$ is replaced with the area of the Venturi throat $\left(A_v\right)$ and the β_o ratio with β_v which is the ratio of throat diameter to pipe diameter.

$$\dot{m}_L = \left[\frac{C_d A_v Y F_a}{\sqrt{1-\beta_v^4}}\right]\sqrt{2\rho_L \Delta P} \tag{2.16}$$

2.1.2.2 Two-phase flow through a Venturi

When Venturis are used to meter wet gas, Stewart et al. (2002) observed that the differential pressure for two-phase flow is greater than it was for single-phase gas flow. This often leads to an "over-reading" of gas flow rate values. Some of the factors that are known to affect this phenomena include liquid fraction, gas velocity, throat-to-pipe diameter ratio and the operating pressure. Lide et al. (2007) evaluated the performance of eight different correlations that are commonly used for Venturis. They found that the gas pressure, throat-to-pipe diameter ratio and the gas velocity played a significant role in the "over-reading" of the meter. The uncorrected Over-reading (OR) is defined mathematically by Eq. 2.17,

$$OR = \frac{\dot{m}_G{}'}{\dot{m}_G} = \sqrt{\frac{\Delta P_{TP}}{\Delta P_G}} \tag{2.17}$$

where $\dot{m}_G{}'$ is the apparent gas mass flow rate and $\dot{m}_G$ is the actual gas mass flow rate.

Some of the models discussed below provide different correlations to calculate OR, which can further be used to determine the actual gas mass flow rate $\left(\dot{m}_G\right)$.

$$\dot{m}_G = \frac{\dot{m}_G{}'}{OR} \tag{2.18}$$

2.1.2.2.1 Homogeneous model

Homogeneous model for single-phase flow can be modified for two-phase flow by using an equation to calculate the average density of two-phase flow (Eq. 2.19) (Lide et al., 2007).

$$\frac{1}{\rho_{TP}} = \frac{x}{\rho_G} + \frac{(1-x)}{\rho_L} \tag{2.19}$$

$$OR = \frac{1}{x}\sqrt{\frac{\rho_L}{\rho_G} + x\left(1 - \frac{\rho_G}{\rho_L}\right)} \tag{2.20}$$

2.1.2.2.2 Smith and Leang Correlation

By taking into account the partial blockage of pipe area by liquid, Smith and Leang (1975) proposed a correlation for Orifice plates and Venturis which corrects for the error caused by liquid by introducing a correction factor, BF, which is a function of mass flow quality.

$$OR = \frac{1}{BF} = \frac{1}{0.637 + 0.421x - \frac{0.00183}{x^2}} \tag{2.21}$$

2.1.2.2.3 De Leeuw correlation

De Leeuw (1997) observed that the error induced by the liquid depends on gas Froude number in addition to pressure and Lockhart-Martinelli parameter. Therefore, he presented a correlation by modifying the Chisholm model by introducing a new parameter, n, which is a function of gas Froude number (Fr_G).

$$Fr_G = \frac{U_{SG}}{\sqrt{gD}}\sqrt{\frac{\rho_G}{\rho_L - \rho_G}} \tag{2.22}$$

$$n = \begin{cases} 0.41 & 0.5 \le Fr_G \le 1.5 \\ 0.606\left(1 - e^{-0.746 Fr_G}\right) & Fr_G \ge 1.5 \end{cases} \tag{2.23}$$

$$OR = \sqrt{1 + X\left(\left(\frac{\rho_L}{\rho_G}\right)^n + \left(\frac{\rho_G}{\rho_L}\right)^n\right) + X^2} \tag{2.24}$$

2.1.2.2.4 Steven correlation

Using a 150 mm Venturi with $\beta = 0.55$, Steven (2002) developed a new empirical correlation by testing the Venturi at 2.0, 4.0 and 6.0 MPa with liquid fractions ranging from 1% to 5% and gas flow rates varying from 400 m^3/h to 1000 m^3/h. The correlation and the empirical constants are given by the following equations.

$$OR = \frac{1 + AX + BFr_G}{1 + CX + DFr_G} \tag{2.25}$$

$$\begin{aligned} A &= 2454.51\left(\frac{\rho_G}{\rho_L}\right)^2 - 389.568\left(\frac{\rho_G}{\rho_L}\right) + 18.146 \\ B &= 61.695\left(\frac{\rho_G}{\rho_L}\right)^2 - 8.349\left(\frac{\rho_G}{\rho_L}\right) + 0.223 \\ C &= 1722.917\left(\frac{\rho_G}{\rho_L}\right)^2 - 272.92\left(\frac{\rho_G}{\rho_L}\right) + 11.752 \\ D &= 57.387\left(\frac{\rho_G}{\rho_L}\right)^2 - 7.679\left(\frac{\rho_G}{\rho_L}\right) + 0.195 \end{aligned} \tag{2.26}$$

2.1.2.2.5 Zhang model

By making corrections to the homogeneous model, Hong-jian et al. (2005) proposed a semi-empirical correlation for Venturis to determine K_L and x, for a low quality oil–air flow.

$$K_L = \frac{1}{\sqrt{c\left(\frac{\alpha}{1-\alpha}\right)^n \left(\frac{\rho_L}{\rho_G}\right)^m + 1}} \tag{2.27}$$

$$x = c'\left(\frac{\alpha}{1-\alpha}\right)\left(\frac{\rho_G}{\rho_L}\right)^H \tag{2.28}$$

The empirical constants c, n, m, c' and H are dependent on the test conditions and flow patterns which are given in Table 2-3.

Table 2-3 *Empirical coefficients for different flow patterns*

Flow pattern	c	n	m	c'	H
Slug flow	0.5	0.95	0.02	0.51	0.65
Wavy flow	1.3	1.15	0.08	1.25	0.70
Annular flow	1.2	0.95	0.05	1.21	0.95

Usually, Venturi meters are coupled with other devices operating on a different measuring principle to determine mass flow rate and mass quality simultaneously. However, Xu et al. (2003) devised a new method to determine mass flow rate by mapping the fluctuation of differential pressure signal of a Venturi with that of mass flow quality, thus eliminating the need for another device.

2.1.2.3 Comparison of two-phase correction factor with gas fraction for orifice and Venturi models

Using Eqs. 2.8, 2.9 and 2.27, Figure 2-3 illustrates the prediction of K_L versus α for the two orifice correlations as well as a Venturi correlation under multiple flow conditions. It was observed that, for both Venturi and orifice models, the two-phase correction factor values are less than one. The predicted K_L under different flow regimes varies considerably. While the addition of ethanol to the current system will affect the flow pattern transitions and will lead to increased formation of small bubbles/homogenous flow, previous work by Triplett et al. (1999) suggests that the flow pattern would transition between bubbly flow (for α < 15%) to plug flow (for α between 15-75%), to annular/churn flow (for α > 75%) over the range of conditions tested. Within a Venturi, the annular and wavy flow appears to have comparable K_L values while transition to slug results in a significant variation in K_L versus α. Similarly, for orifice models depending on the approach taken, significant variations in the prediction of K_L can be observed.

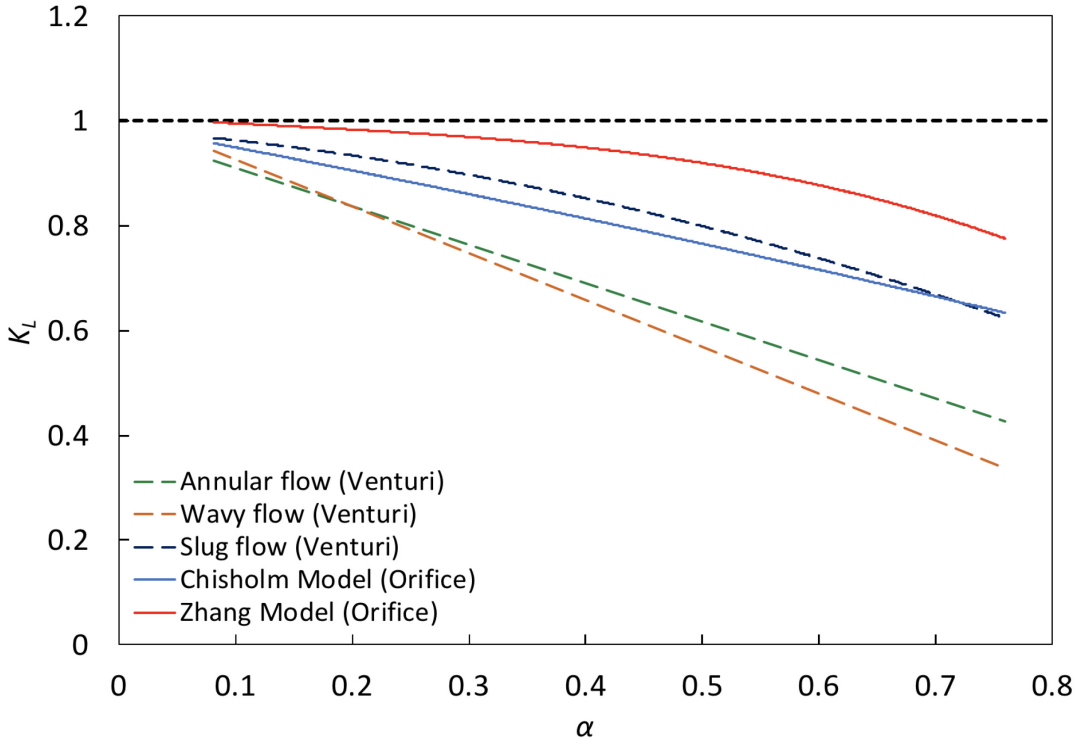

Figure 2-3 *K_L versus α for Orifice plates and Venturi nozzles*

2.2 Coupling method

In order to characterize the individual flow rates of gas and liquid, flow measurement devices are typically coupled with another device measuring void fraction or density. Some of the combinations investigated by different authors are listed in Table 2-4.

Table 2-4 *Combination of flowmeters investigated to measure multiphase flow (Xing et al., 2014)*

Single-sensor		Venturi (Fincke et al., 1999; Xu et al., 2003; Xu et al., 2011) Swirl meter (Hua and Geng, 2012)
Double-sensor	Two flow sensors	Venturi plus Venturi (Dualstream, 2001) Venturi plus V-cone (Xu et al., 2013) V-cone plus V-cone (Zhang et al., 2010) V-cone plus shuttle cone (He et al., 2013) Slotted orifice plus slotted orifice (Li et al., 2009; Yanfeng et al., 2007) Slotted orifice plus swirl meter (Hua and Geng, 2013) Venturi plus turbine meter (Huang et al., 2007) Venturi plus vortex meter (Sun, 2010)
	Flow sensor plus phase fraction sensor	Venturi nozzle plus capacitive sensor (dos Reis and Goldstein Jr, 2008) Venturi plus ECT (Hong-jian et al., 2005; Huang et al., 2005) Venturi plus ERT (Meng et al., 2010) Venturi plus microwave probe (Bø et al., 2002) Venturi plus sonar (Gysling et al., 2007) Ultrasonic and Coriolis meter (Xing et al., 2014)

2.3 Phase holdup measurement devices

The technologies that are more commonly used to measure the void fraction in a multiphase flow are gamma-ray attenuation and electrical impedance techniques. These techniques are discussed further in the following sections.

2.3.1 Gamma-ray methods

Gamma-ray densitometry is preferred for MPFM over other meters for the following reasons

- Non-intrusive sensors
- No detector corrosion
- No pressure drop across the instrument
- Zero impact on fluid flow

A radioactive source, usually Caesium-137 and thulium-170, is used to emit a thin beam of gamma rays with an initial intensity of I_o. This gamma ray emission passes through the multiphase flow mixture sandwiched between two walls before the resultant intensity (I_d) is determined by a collimated detector (Figure 2-4). While it passes through the multiphase flow, the attenuation of gamma beam takes place due to photoelectric effect, pair production and Compton effects. The initial and final intensities of the gamma ray are recorded and are used to determine the void fraction of the multiphase flow (Åbro and Johansen, 1999; Falcone et al., 2009).

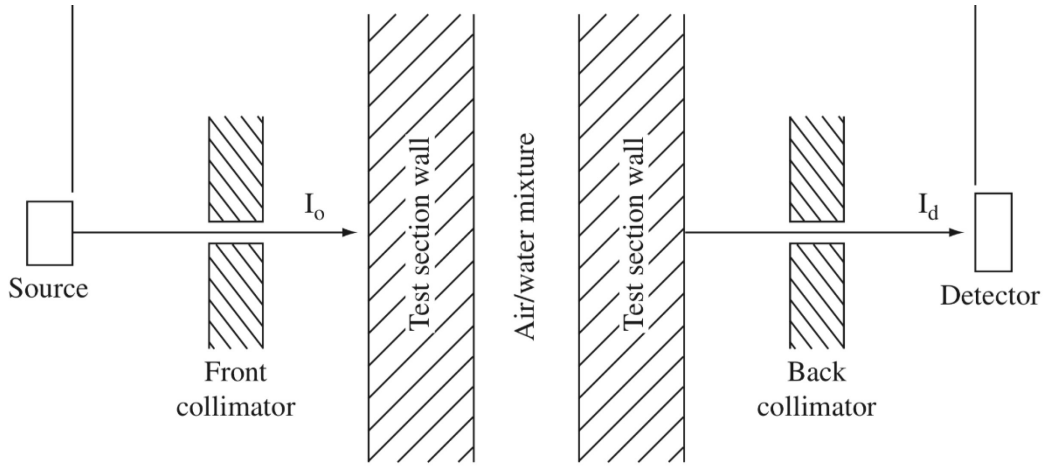

Figure 2-4 *Experimental setup for Gamma-ray densitometry (Falcone et al., 2009)*

Roshani et al. (2015) developed a method based on gamma-ray attenuation using artificial neural networks (ANN) to establish the flow regime and estimate the gas fraction in gas-liquid flows. They simulated the ANN for stratified, homogeneous and annular flow regimes using Monte Carlo N-particle (MCNP) code and tested the annular regime experimentally. Using this method, they were able to identify the flow regime with a 100% accuracy and were able to predict the gas fractions with errors less than 1.1% for two-phase flows with gas fractions ranging from 5% to 95%.

Tjugum et al. (2002) used multi-beam gamma-ray densitometry to establish the flow regimes in three-phase flow. A special tilt section was designed and built to perform experiments on deviated three-phase flow with oil, water and gas phases. They were able to demonstrate that several collimated detectors and a fan beam geometry with a single radiation source is enough to yield information on the distribution of gas and liquid in multiphase pipe flow. Different flow regimes were identified successfully, and the acquired flow regime information was used to enhance the accuracy of the void fractions.

Åbro et al. (1999) used a ^{241}Am source and EGS4 software package to identify the flow regime and determine the phase fraction in oil/gas pipes. Simulations were performed for

homogenous, annular and stratified flows and for void fractions ranging from 0 to 100%. The simulated data was then used to train neural networks to distinguish the flow regimes accurately and to determine the void fractions with an error of 3% for all flow regimes.

2.3.2 Electrical impedance methods

The phases in the multiphase flows have significantly different electrical impedances. Various probes can be designed to measure the resistance, capacitance, inductance or a combination of them to determine the void fraction of gas flowing in a multiphase flow. The impedance can be measured for a large volume using an integrated probe or for a small region using a local probe. The advantages of using impedance probes are high frequency response, low cost and ease of construction (Ceccio and George, 1996).

Paranjape et al. (2012) developed a custom-designed electrical impedance meter to determine the phase fraction of two-phase flow in micro-channels by using the variation in permittivity and the specific electrical conductance of the individual phases. To identify the flow regimes, a Kohonen self-organizing map is used.

Huang et al. (2003) proposed a new method to measure the phase fraction of two-phase flow using a 12-electrode electrical capacitance tomography measurement system. A new image reconstruction algorithm was developed using algebraic reconstruction technique algorithm and Tikhonov regularization principle. The errors in phase fraction measurement for different flow regimes was less than 5%.

2.3.3 Other technologies

Some other technologies available for MPFM are acoustic attenuation, neutron interrogation, microwave attenuation and infrared spectroscopy (Falcone et al., 2009). A brief review of multiphase flow metering techniques is given by Rajan et al. (1993). Some of the more recent techniques developed for MPFM are nuclear magnetic resonance

spectroscopy, particle image velocimetry and a multisensory intelligent device using electrical and acoustic sensors (Bilgic et al., 2015; Lindken and Merzkirch, 2002; Meribout et al., 2010).

2.4 Coriolis meter for multiphase flow metering

In the recent decade, Coriolis meter has gained a lot of importance in multiphase flow metering, particularly in the oil and gas industry. Coriolis meter is preferred over other flow meters because of its accuracy, reliability and its ability to measure mass flow and density simultaneously (Gysling, 2007; Wang and Baker, 2014). In the Coriolis meter, the fluid passes through one or more tubes which oscillate at a certain frequency when the fluid passes through them. The mass flow rate and density of the fluid passing through can be determined from the frequency of this oscillation (Anklin et al., 2006; Henry, 2008; O'Banion, 2013). The Coriolis meter is "almost perfect" for homogeneous flow providing the mass flow rate measurements with an accuracy of ±0.2%; however, the measurement errors increase considerably with introduction of even small amounts of gas (Liu et al., 2001; Reizner, 2003). But in the recent years, significant progress has been made in this area and numerous models were proposed to reduce the errors in mass flow rate and density values.

Liu et al. (2001) developed a digital Coriolis transmitter for two-phase flow and proposed a neural network-based solution to correct the measurements of mass flow rate. Using this method, the mass flow rate errors were reduced from 20% to 2%. Henry et al. (2006) have proposed an empirical methodology to develop correction models for a given two-phase flow mixture and Coriolis flow tube for gas void fractions reaching up to 80%. Corrected measurements were within 1-5% of actual mass flow and density values. The results were validated by conducting field trials using heavy oil.

Xing et al. (2014) developed a combination measurement method using ultrasonic and Coriolis flowmeters to measure the mass flow rates of individual phases in a two-phase

flow. They developed a coupling model using the ultrasonic flowmeter to measure the apparent volumetric flow rate of gas and the mass flow rate from Coriolis meter and found that the root-mean-square (RMS) errors were 3.09% and 12.78% for gas and liquid mass flow rates respectively. In addition to that, they also developed another coupling model using density instead of mass flow rate and determined the RMS errors to be 2.59% and 4.38% for gas and liquid mass flow rates respectively.

Attempts have also been made by Henry et al. (2013) to apply Coriolis meters in three-phase flow applications. This was achieved using a commercial water cut meter, where mass flow and density were measured using a Coriolis meter, pressure and temperature were measured by gauges, and water cut was determined from a water cut meter. All these parameters are used to model three-phase flow and determine the flow rates of individual components. The liquid mass flow and gas mass flow errors were contained to ±2.5% and ±5% respectively.

In this thesis, a Coriolis meter was used as a standard to compare the results obtained with the developed pressure drop based metering device.

2.5 Flow expansion of compressible fluids

Although non-intrusive, gamma-ray densitometry requires proper homogenization of the multiphase flow. In addition to that, the materials used to generate gamma-rays are radioactive, so proper care is required while handling the materials. As for electrical impedance techniques, the capacitance/conductance probes are susceptible to different kinds of corrosion. In order to avoid these issues, the compressibility of two-phase flow at low-pressure conditions can be used to determine the void fraction within an air/water/ethanol stream. This work explores the use of a static mixer with alternating 90-degree constrictions to homogenize the flow while measuring pressure drop. By maintaining a consistent homogenized flow regime, the flow patterns effects on K_L values can be minimized. Through the introduction of an additional pressure drop between two of

these static mixers using a gate valve, a change in gas fraction can be produced which would result in a difference in K_L values applicable in each meter. By charactering the dependence of K_L on α, both mass flow rate (which should be constant in each of the meters) and α can be approximated. The following chapter explores the experimental applications of this principle, characterizing the single-phase and multiphase flow rates along with the phase holdup.

Chapter 3 EXPERIMENTAL DESIGN

3.1 In-line phase monitoring for an ebullated bed reactor

The fundamental drive for this research project was the need to do in-line phase monitoring of a gas-liquid emulsion foam in an ebullated bed reactor (EBR) (Figure 3-1). As part of a large project with Syncrude Canada looking at phase separation in an ebullated bed, the conditions in the recycle line were investigated. Our initial approach was to send the two-phase mixture from the recycle line into a two-phase separator where the liquid flow was measured using a liquid flow meter and the gas flow was measured using a mass flow meter. The same procedure was applied to measure the different phases obtained in the exit stream from the top of the reactor. The intention was to separate the phases, measure them individually, combine them and send the mixture back to the reactor. The experimental setup with the separators and the corresponding flow diagram are illustrated in Figures 3-2 and 3-3.

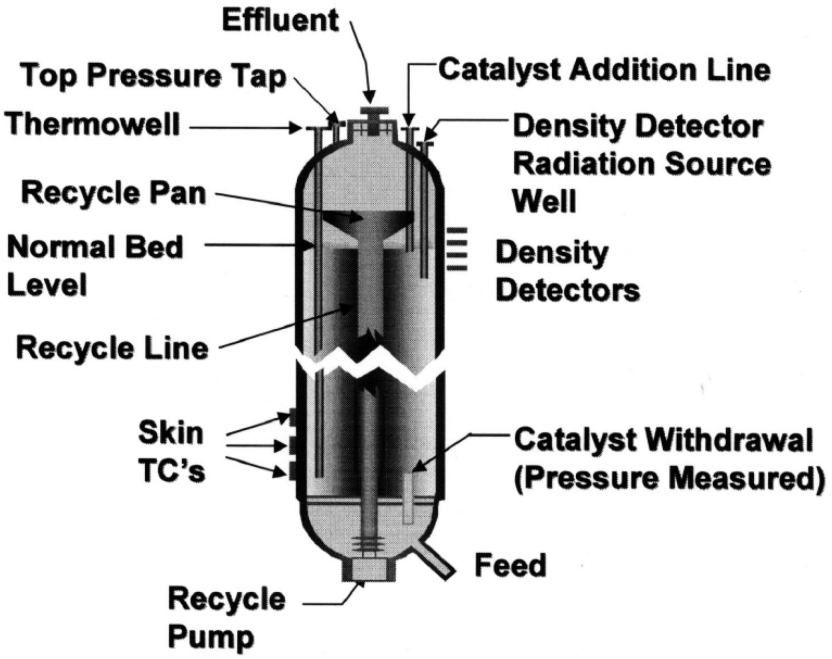

Figure 3-1 *Schematic of a standard LC-Finer ebullated bed reactor (McKnight et al., 2008)*

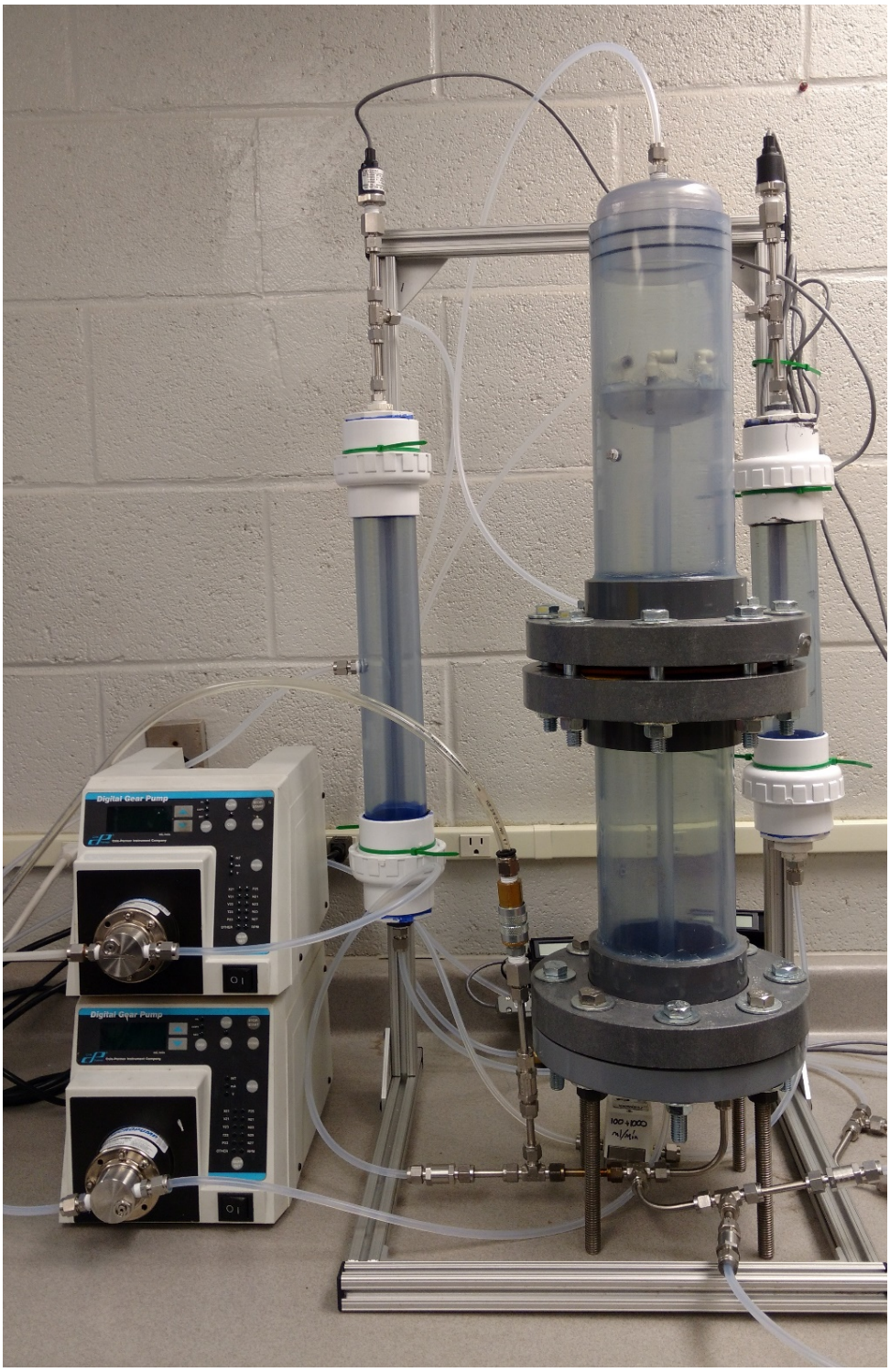

Figure 3-2 *A miniaturized version of ebullated bed reactor used for the experiment. Feed and recycle pumps (left) circulate fluid through the ebullated bed (right front), with the recycle line passing through the left separator and the top of the reactor passing through the right separator.*

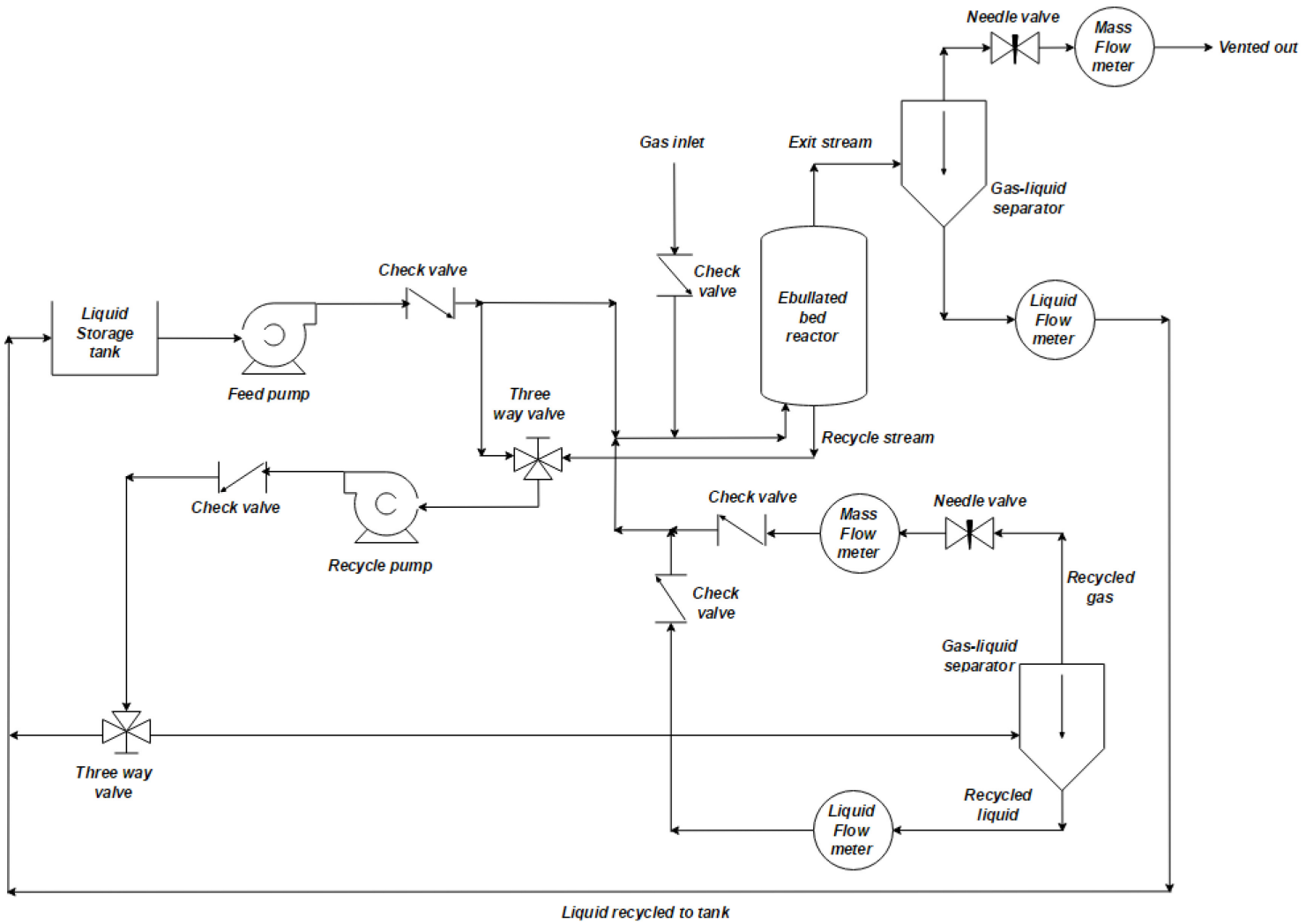

Figure 3-3 *Experimental setup of the system with EBR*

However, upon completion of this design it was found that the separation was unstable, the fluid flow gained a pulsing format and the flow conditions inside the column changed significantly. In a commercial reactor, they do not separate these phases which led us to explore multiphase in-line metering technology. So, in order to do this, a pressure drop based metering device was developed and correlations between the measured pressure drops and the mass flow rate of the multiphase flow were proposed.

3.2 Dual-pressure drop element (DPDE) device

The flow metering system developed in this work, named dual-pressure drop element (DPDE) device, consisted of two pressure drop elements or static mixers separated by a larger flow restriction intended to generate sufficient energy dissipation to ensure that the gas density varied between the first and second elements (Figure 3-4). Each of the static mixers was produced to have ~2.5 psig pressure drop at a liquid flow rate of 0.096 m^3/h. Due to the variability in the production method, this resulted in the upstream mixer having 5 constrictions and the downstream mixer having 4 constrictions. The constrictions were generated by crimping a 1/4 inch stainless-steel tube at 1 cm intervals with a 90-degree rotation between the constrictions. The impact of the number of constrictions was accounted for in the single-phase calibration of each mixer. Two-phase flow was generated using a calibrated P35 Micro pump (GB-P35.JVS.A.B1) driven by a Micro pump 75211-30 controller and a gas mass flow controller (Omega FMA1816A). Water containing 0.5% ethanol was used as the liquid phase, where the ethanol served as a surfactant to produce an effervescent foam in regions of high agitation. Air was introduced through the branch of a Swagelok T fitting, with the T having an internal diameter of 1/8 inch. The gas/liquid flow profile was allowed to develop over a length of ~10 cm prior to entering the first static mixer. It was expected that at the range of gas/liquid flow rates tested, the flow profile would have varied from bubbly to plug/slug to slug/churn, and eventually wavy annular/annular flow. The absolute pressures and pressure drop across both the upstream and downstream flow elements were monitored using ProSense SPT25-10-0060D, SPT25-10-V30A and Omega PX409-005DWUV transducers and recorded via an NI DAQ system powered by LabVIEW. Fluid temperature and density were confirmed at multiple times

during the experiment using an Anton Paar DMA 35 portable density meter, in addition to the measured values obtained from the Emerson CMF025M Coriolis meter installed following the last pressure drop element. Backpressure within the system was controlled via a needle valve located after the Coriolis meter.

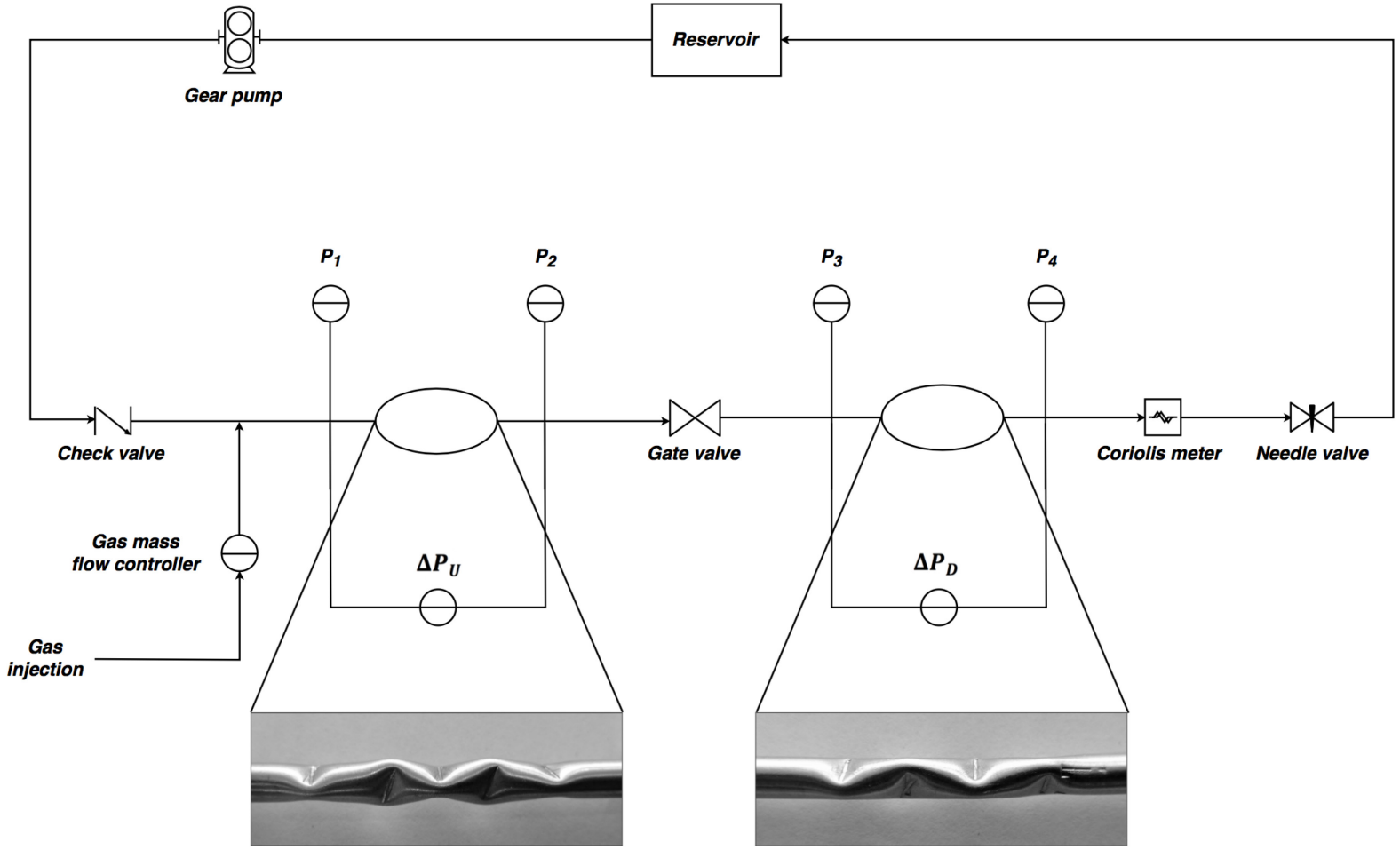

Figure 3-4 *Flow diagram for the pressure drop based metering device*

3.3 Corrections for density

For the purpose of all calculations, the density of gas and liquid are necessary. The density of the liquid has to be corrected to account for the changes in temperature. The density-temperature correlation (Eq. 3.1) was derived from published density values for water and was validated with Coriolis meter measurements for the single-phase flow. T is the temperature of fluid in °C.

$$\rho_L = -0.25T + 1003.838 \tag{3.1}$$

The gas was assumed to expand isothermally due to the significant thermal mass of the liquid and hence ideal gas law was used to estimate ambient air density. As a reference point, the pressure and temperature of the air was assumed to be at 101325 Pa and 25 ºC respectively. Note that the temperature variation was minimal within the context of the experiment.

$$\rho_{G,conditions} = \rho_{atm}\left(\frac{P_{conditions}}{P_{atm}}\right) \tag{3.2}$$

3.4 Corrections for viscosity

Similarly, the viscosity of liquid was also corrected by developing a viscosity-temperature correlation (Eq. 2.3) using literature values for water. T is the temperature of fluid in °C and μ_L is the viscosity of liquid in kg/m·s. It was assumed that the viscosity of gas varied minimally and for all calculations concerned viscosity of liquid is used including those of multiphase flow.

$$\mu_L = \frac{1.4641 - 0.0229T}{1000} \tag{2.3}$$

Chapter 4 RESULTS AND DISCUSSION

4.1 Flow system calibration

Prior to carrying out this research study, both the gas and liquid systems were calibrated. The liquid flow rate leaving the metered gear pump was calibrated to account for RPM and backpressure effects, with correlations developed to determine the liquid mass flow rate. The Coriolis meter which gives a high degree of confidence for the measurement of single-phase flow was used, where the back pressure of the outlet of the pump was varied by restricting the flow through the needle valve.

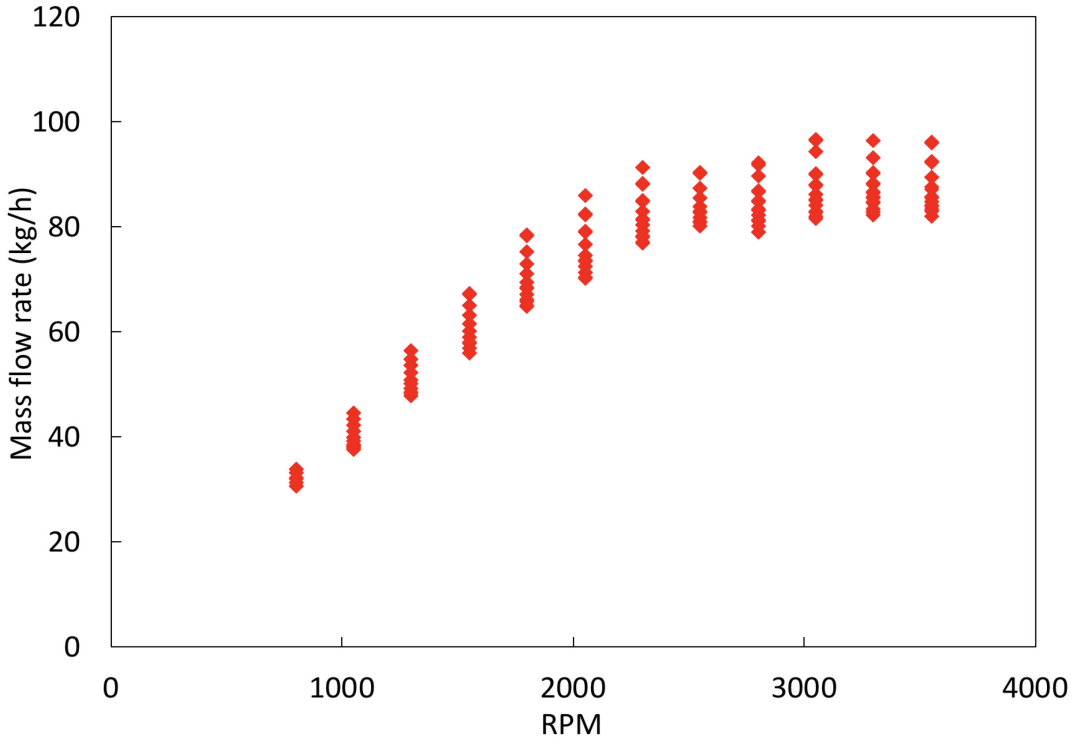

Figure 4-1 *Mass flow rate as a function of RPM. Vertical variation is due to changes in backpressure at a set RPM*

Through the regression of the flow rate as a function of absolute pressure P_1, the equations given in Table 4-1 provided an estimate for the mass flow rate of liquid at different set RPMs.

Table 4-1 *Mass flow rate equations developed for different RPMs*

RPM of the pump	Mass flow rate equation used
800	$\dot{m}_{L,800} = -1.327P_1 + 37.942$
1050	$\dot{m}_{L,1050} = -1.234P_1 + 50.889$
1300	$\dot{m}_{L,1300} = -1.166P_1 + 64.962$
1550	$\dot{m}_{L,1550} = -1.252P_1 + 79.991$
1800	$\dot{m}_{L,1800} = -1.586P_1 + 100.300$
2050	$\dot{m}_{L,2050} = -2.165P_1 + 122.420$
2300	$\dot{m}_{L,2300} = -2.557P_1 + 138.270$
2550	$\dot{m}_{L,2550} = -2.727P_1 + 146.430$
2800	$\dot{m}_{L,2800} = -2.587P_1 + 143.890$
3050	$\dot{m}_{L,3050} = -2.892P_1 + 155.520$
3300	$\dot{m}_{L,3300} = -2.684P_1 + 151.230$
3550	$\dot{m}_{L,3550} = -2.559P_1 + 148.600$

The liquid density determined from the Eq. 3.1 corresponded quite well with the predicted liquid densities obtained from the Coriolis meter.

For all gas density calculations, the actual density has been corrected for the pressure at which the density and mass flow rate measurements occurred. For the Coriolis meter, the densities were calculated using pressure at P_4 and the average pressure at the middle of the

Coriolis meter (Eq. 4.1). The pressure drop across the Coriolis meter $\left(\Delta P_{Coriolis}\right)$ was determined by applying a linear correlation between mass flow rate and pressure drop, where the nominal flow rate (1310 kg/h) across the meter for one bar was known. For the DPDE device, the actual gas density has been determined based on the average pressure between P_1 and P_2 for the upstream section (Eq. 4.2), and the average pressure between P_3 and P_4 for the downstream section (Eq. 4.3). Gas fraction estimates were also corrected for pressure effects and expansion.

$$\rho_G = \rho_{atm}\left(\frac{P_4 - \left(\Delta P_{Coriolis}/2\right)}{P_{atm}}\right) \tag{4.1}$$

$$\rho_{G,U} = \rho_{atm}\left(\frac{\left(\left(P_1 + P_2\right)/2\right)}{P_{atm}}\right) \tag{4.2}$$

$$\rho_{G,D} = \rho_{atm}\left(\frac{\left(\left(P_3 + P_4\right)/2\right)}{P_{atm}}\right) \tag{4.3}$$

4.2 Coriolis meter

All experiments were carried out concurrently where the flow was varied from 800 RPM (0.033 m^3/h) to 3550 RPM (0.096 m^3/h) in increments of 250 RPM, while the gas flow rate for each RPM varied from 0 LPM (0 m^3/h) to 2 LPM (0.117 m^3/h) in increments of 0.25 LPM. While the Coriolis meter was in place, experiments were conducted to compare the mass flow rate and density approximations against the values obtained from metering.

Measurements from the DPDE device were also taken concurrently for direct comparison with the Coriolis meter.

With the Coriolis meter in place, the liquid was allowed to enter the system until there are no gas bubbles in the loop. After the flow was fully-developed, gas was injected into the system and allowed to run freely through the system. After steady-state was achieved, the data was recorded for 60 seconds for three trials. The same process was repeated for every increment of liquid and gas flow rates.

The mass flow rate and density measurements from the Coriolis meter were taken manually. The measurements for each trial were taken over a course of a few minutes. During that time period, the lower bound, the higher bound and the value which appeared to be the frequent center of fluctuations was recorded for both mass flow rate and density. The average of the three values was used as the mass flow rate and density of the multiphase flow obtained from Coriolis meter.

4.2.1 Variation in mass flow rate measurements

The relative standard deviation (RSD) of the mass flow rate measurements determined from the Coriolis meter for increasing gas fractions is illustrated in Figure 4-2. The introduction of even small quantities of gas into the system resulted in an increase of RSD values from near-zero to values ranging from 5 to 35% depending on the gas fraction present. RSD is defined by Eq. 4.4.

$$RSD = \frac{\text{Standard deviation} \times 100}{\text{Average}} \tag{4.4}$$

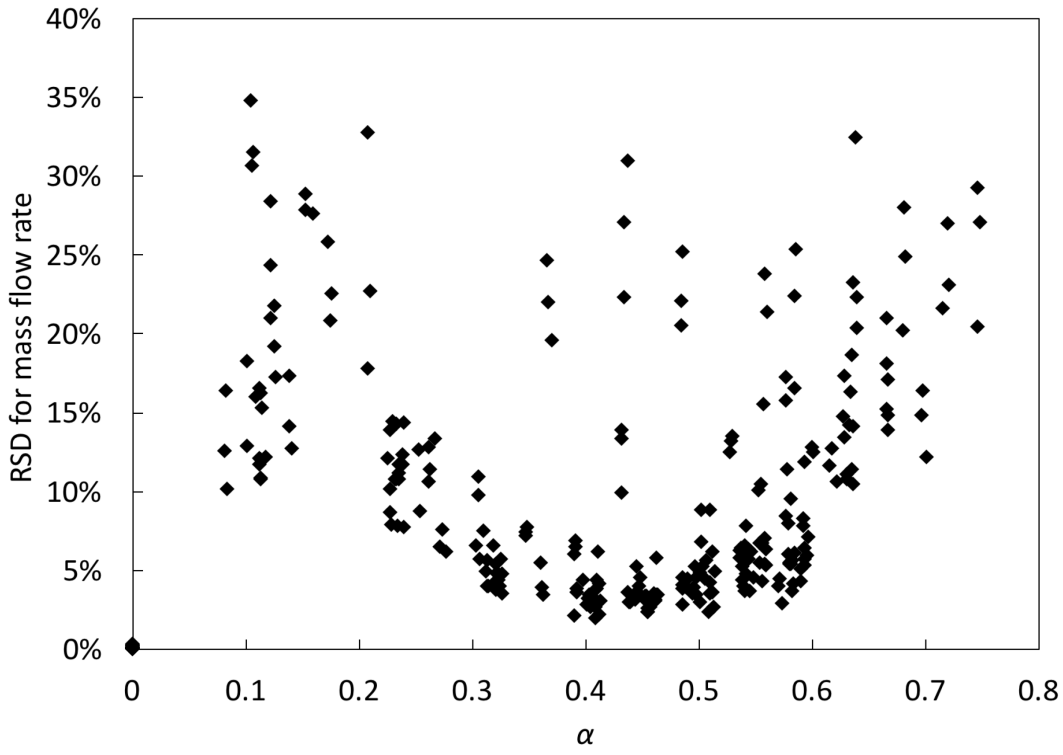

Figure 4-2 *Relative standard deviation for mass flow rate varying with gas fraction*

As gas was introduced into the system, it was more challenging to maintain a homogeneous flow pattern for low gas flow rates and high gas flow rates. More variability in mass flow rates was observed at low and high gas fractions which was assumed to be because of dispersed bubble flow pattern at low gas flow rates and annular or slug flow patterns at higher gas flow rates.

4.2.2 Mass flow rate performance

The average mass flow rate was well-predicted for single-phase (Figure 4-3, red symbols). However, with the onset of multiphase flow through the Coriolis meter, significant variation was observed in the measured value. For mass flow rate, it varied by as much as ±30 kg/h with about 90% of the data falling in ±20 kg/h range for intermediate gas flow rates.

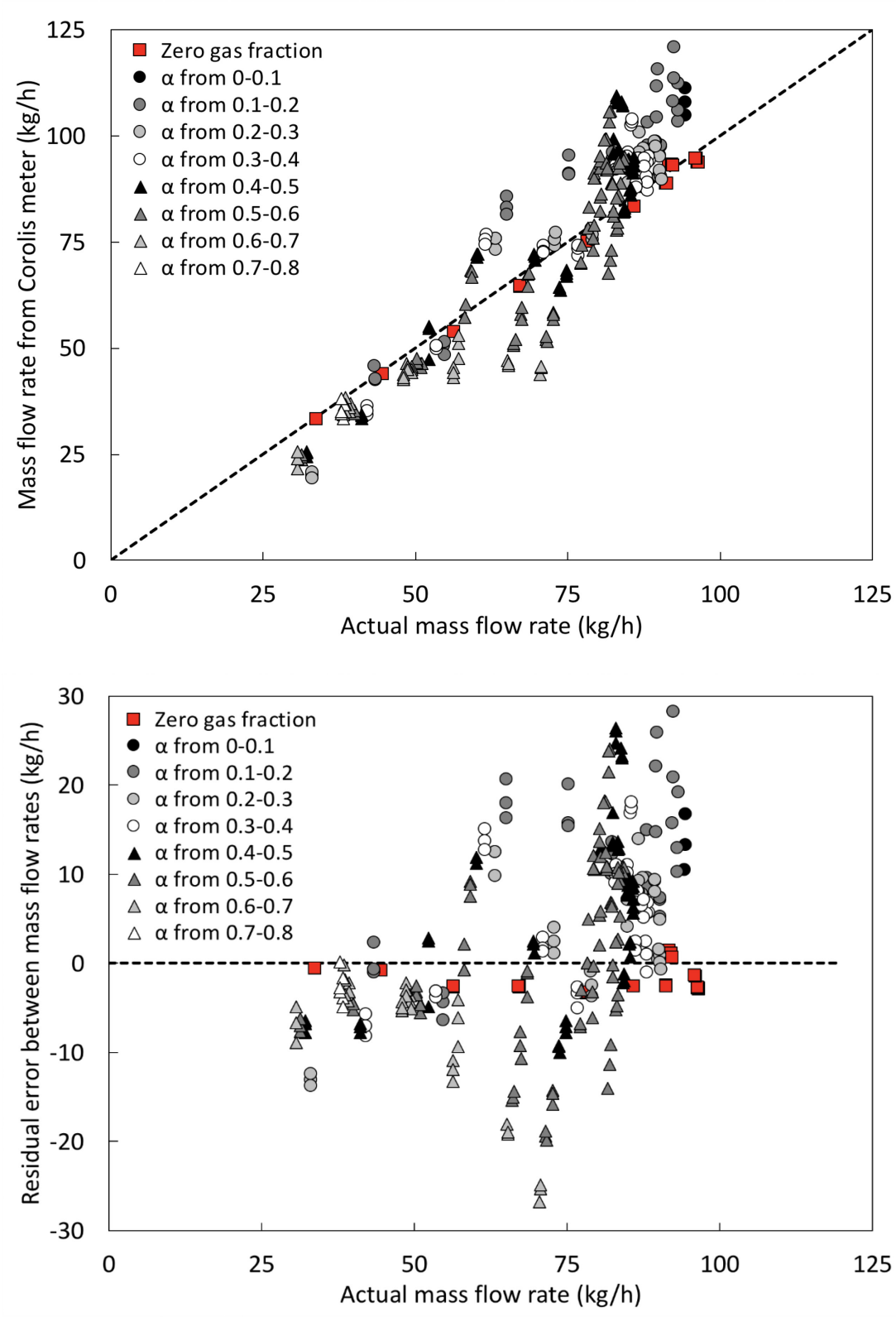

Figure 4-3 *Comparison of mass flow rate from Coriolis meter and actual mass flow rate (top) and the residual errors between them (bottom)*

4.2.3 Variation in density measurements

RSD of density measurements determined from the Coriolis meter are illustrated in Figure 4-4. For single-phase flow, density estimates were consistent with measurements obtained using the DMA 35 portable density meter. However, it should be noted that RSD values were relatively high at lower and higher gas fractions compared to those at intermediate gas fractions. It was assumed that the flow patterns were not only affecting mass flow rate but density estimates of two-phase flow as well.

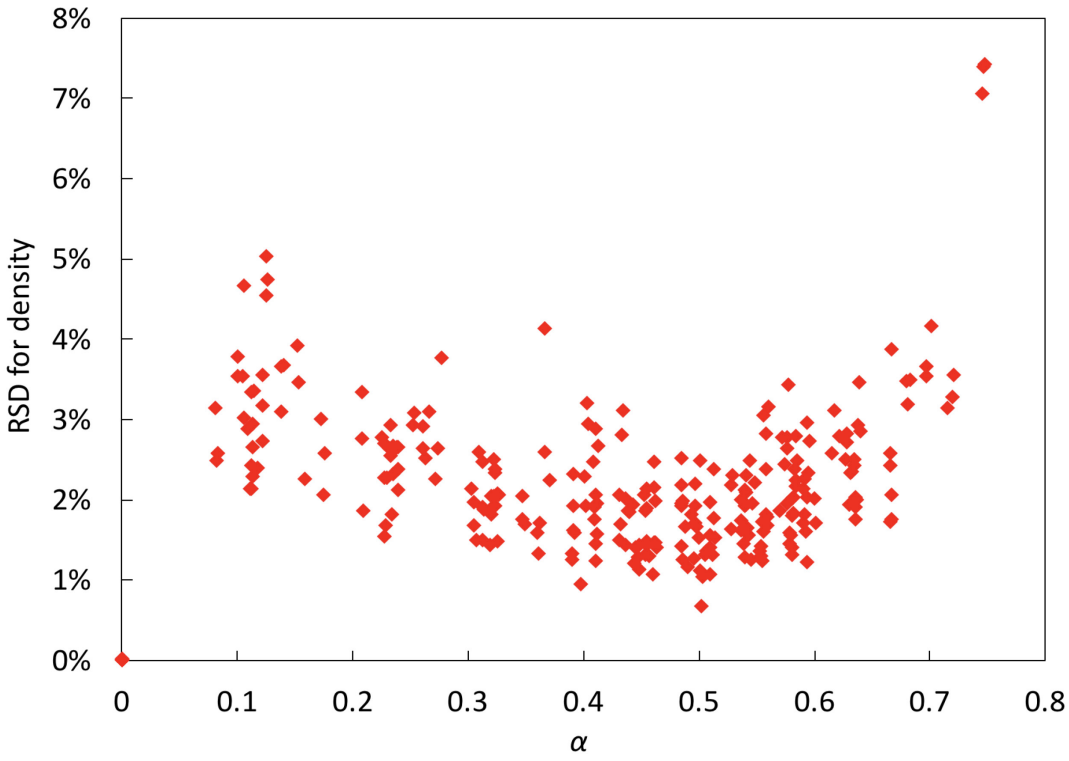

Figure 4-4 *Relative standard deviation for density varying with gas fraction*

4.2.4 Density performance

Since the liquid used for the experiments was an ethanol-water mixture containing mostly water (only 0.5% ethanol), the density measurements for single-phase flow were all clustered around 1000 kg/m^3. However, similar to the trend observed for mass flow rate measurement, the introduction of gas into the system resulted in significant variations in the residual errors (Figure 4-5).

From the residual error data, a variation in densities from -200 kg/m^3 to 50 kg/m^3 with most of the data lying in between -100 to 50 kg/m^3 can be observed. The density values at higher RPMs were more accurately predicted by the Coriolis meter than at the lower RPM values. For example, for gas fractions in between 0.2 and 0.3, the data with near-zero error values was found to have RPM values above 3000. But for lower RPMs, there was a bias towards the underestimation of density. This trend seems to be consistent for all the range of gas fractions tested. Better homogenization of fluids at higher flow rates prior to entering the Coriolis meter could be responsible for this phenomenon.

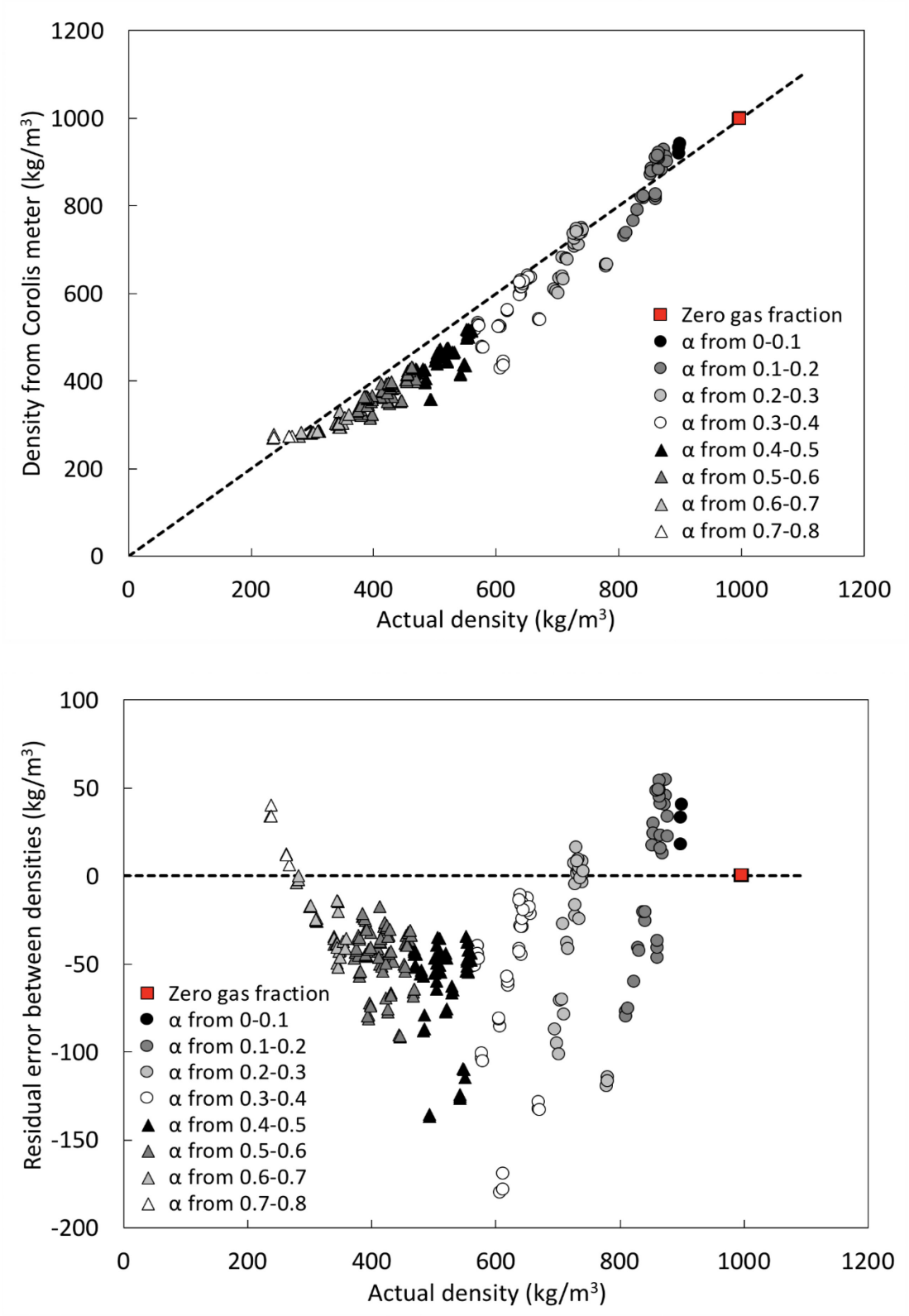

Figure 4-5 *Comparison of density from Coriolis meter and actual density (top) and the residual errors between them (bottom)*

4.3 DPDE device

The following sections give an overview of the methodology used to develop the correlations between pressure drops and mass flow rate of the two-phase flow.

4.3.1 Characterizing the geometry

Using the liquid flow data obtained from the DPDE device, the slope of a plot between mass flow rate of the liquid $\left(\dot{m}_L\right)$ and the pressure drop term $\left(\sqrt{2\Delta P_L \rho_L}\right)$ can be determined for both upstream and downstream pressure drop elements. The slope of the line represents the $\left[\frac{C_d A Y F_a}{\sqrt{1-\beta^4}}\right]$ including the coefficient of discharge $\left(C_d\right)$, area of cross-section $\left(A\right)$, compressibility factor $\left(Y\right)$, thermal expansion correction factor $\left(F_a\right)$ and orifice (or throat)-to-pipe diameter ratio $\left(\beta\right)$.

For a fully-developed turbulent flow through an orifice, C_d remains constant and a plot of mass flow rate of liquid $\left(\dot{m}_L\right)$ versus $\left(\sqrt{2\Delta P_L \rho_L}\right)$ should yield a linear plot with a constant slope. However, it was observed that at lower $\left(\sqrt{2\Delta P_L \rho_L}\right)$ values, mass flow rate values are slightly overestimated when a zero-intercept was applied. In this region, the Reynolds number approaches the traditional transition regime where C_d is expected to decrease. To account for this, a linear plot with a non-zero intercept was used for the purpose of estimating single phase mass flow rate, recognizing that a power-law function could also be applied with similar results obtained.

The mass flow rate for the upstream and downstream sections are determined from Eqs. 4.5 and 4.6, where m_U^*, c_U^* and m_D^*, c_D^* are the slope and intercept values corresponding to upstream and downstream mass flow rate equations respectively. ΔP_U and ΔP_D are the

pressure drops across each of the pressure-based measurement devices. A subsequent plot of the mass flow rate in each of these sections versus $\left(\sqrt{2\Delta P_L \rho_L}\right)$ (Figure 4-6) resulted in values of $m_U^* = 5.066\times10^{-6}\, m^2$ and $c_U^* = -1.352\times10^{-3}\, kg/s$ for the upstream section and $m_D^* = 4.726\times10^{-6}\, m^2$ and $c_U^* = -1.606\times10^{-3}\, kg/s$ for the downstream section.

$$\dot{m}_{L,U} = m_U^* \sqrt{2\rho_L \Delta P_{L,U}} + c_U^* \tag{4.5}$$

$$\dot{m}_{L,D} = m_D^* \sqrt{2\rho_L \Delta P_{L,D}} + c_D^* \tag{4.6}$$

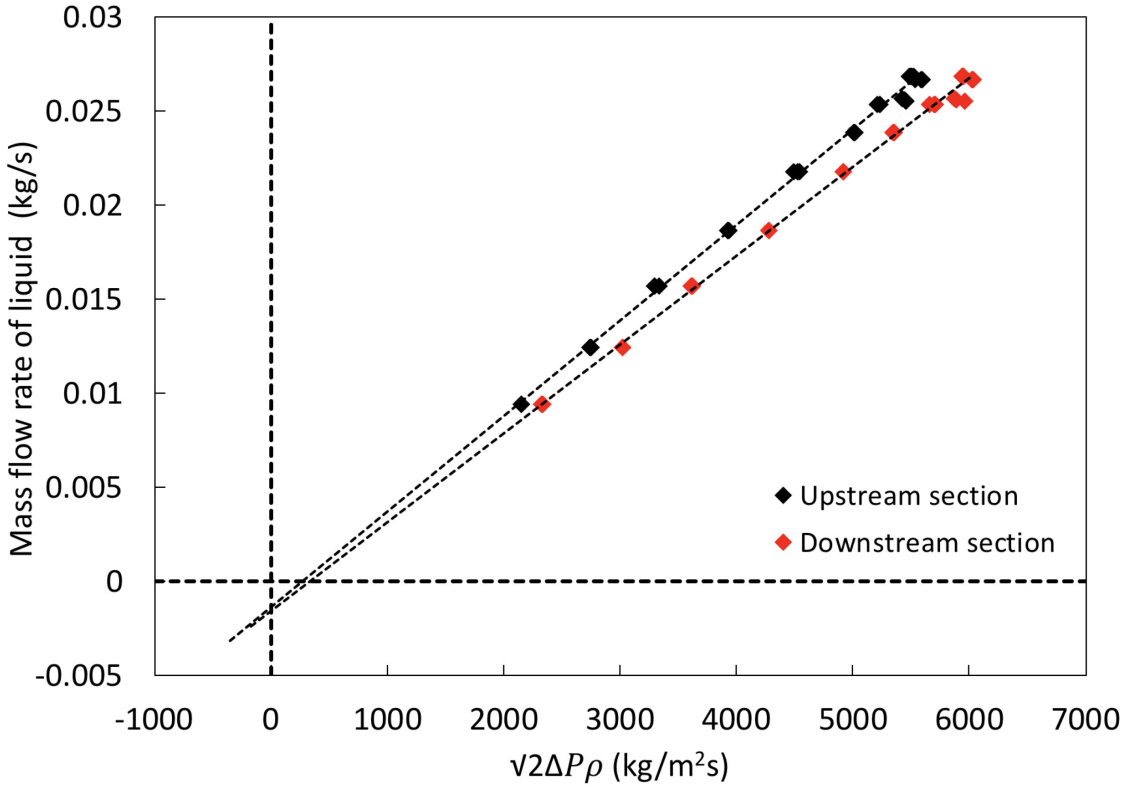

Figure 4-6 *Correlation between mass flow rate and pressure drop for single-phase flow through the upstream and downstream flow restriction elements*

During the experiment, the crimped pipe elements were not altered or changed in any way and remained in the same positions.

To account for the two-phase flow occurrence, necessary corrections were applied to Eqs. 4.5 and 4.6 by introducing a K_L parameter for correlating the mass flow rates of two-phase flow to the pressure drops of two-phase flow.

$$\dot{m}_{TP,U} = K_{L,U}\left(m_U^* \sqrt{2\rho_L \Delta P_{TP,U}} + c_U^*\right) \tag{4.7}$$

$$\dot{m}_{TP,D} = K_{L,D}\left(m_D^* \sqrt{2\rho_L \Delta P_{TP,D}} + c_D^*\right) \tag{4.8}$$

Liquid density is used in Eqs. 4.7 and 4.8 to maintain consistency with single-phase correlations, recognizing the impact of mixture density variation will be included within the K_L parameter. The compressibility coefficient for two-phase flow, $Y_{TP} = 1$ for Mach numbers less than 0.3 (Oliveira et al., 2009), which is consistent with the flow conditions present here. By rearranging Eqs. 4.7 and 4.8, K_L can be isolated and calculated using the measured mass flow rate and corresponding pressure drops for two-phase flow.

$$K_{L,U} = \frac{\dot{m}_{TP,U}}{m_U^* \sqrt{2\rho_L \Delta P_{TP,U}} + c_U^*} \tag{4.9}$$

$$K_{L,D} = \frac{\dot{m}_{TP,D}}{m_D^* \sqrt{2\rho_L \Delta P_{TP,D}} + c_D^*} \tag{4.10}$$

4.3.2 Comparison between different models

Potential models for K_L were described in Chapter 2 and specifically the Chisholm model and the Zhang model have been shown for comparison purposes for our particular system. Using the Homogeneous model, K_L was determined from experimental results using Eqs. 4.9 and 4.10 and is illustrated for conditions in Figure 4-7. Eqs. 2.5 and 2.8 were used to determine the K_L values for Chisholm model and Eq. 2.9 for Zhang model.

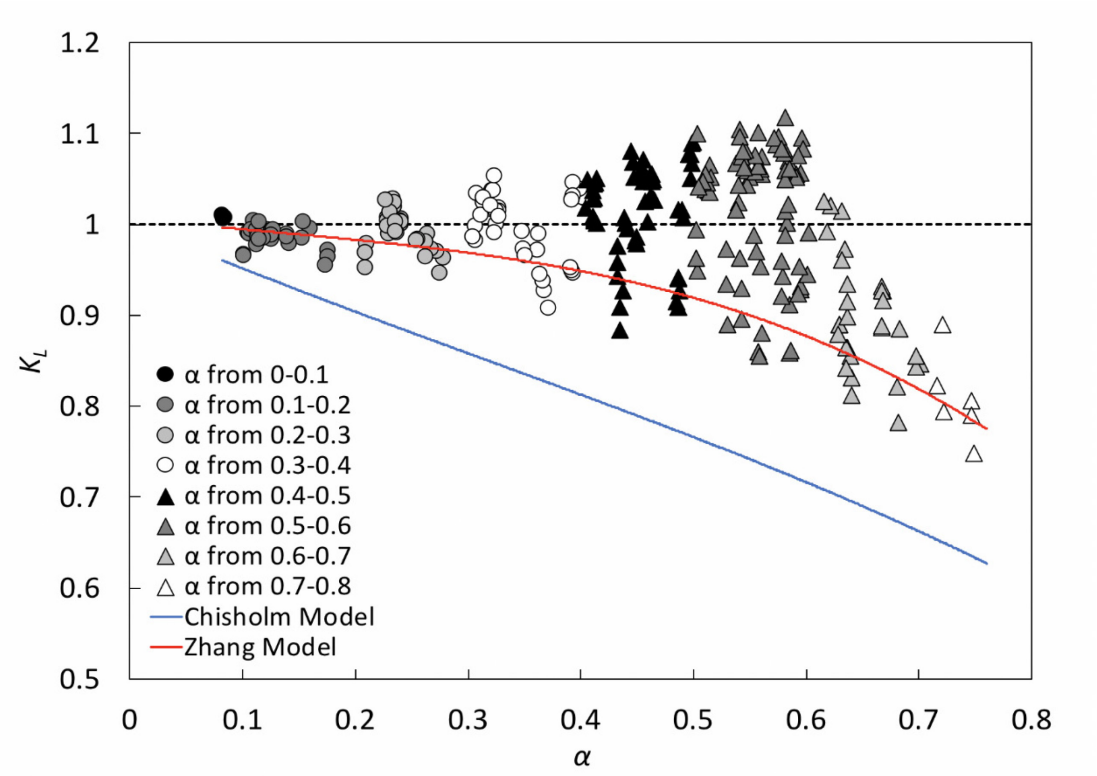

Figure 4-7 *Two-phase correction factor determined from homogeneous flow model for different gas fractions vs predicted K_L from Chisholm and Zhang models*

Ideally, the two-phase correction factor is a sensitive variable to gas fraction, so the pressure drop between metering devices will cause sufficient gas expansion to cause a variation in K_L. If a Venturi is used, it is difficult to obtain a steep function, but it is possible to achieve more pressure recovery compared to an orifice plate. Most existing

models require K_L to be less than one, meaning that pressure drop is higher when multiphase flow is introduced through an orifice relative to single-phase flow at the same mass flow rate. But, for the number of conditions tested, across multiple gas flow rates, values of $K_L > 1$ were observed in these experiments. This suggests either a pressure recovery or streamlining effect being introduced into the current system when multiphase flow is first introduced. Because K_L based models require values of one or less and significant error is introduced using this model for our system, a polynomial based correlation specific to our system was explored.

While developing our own correlation for K_L as a function of gas fraction, it was recognized that having $K_L > 1$ is different from the majority of published literature on orifice-based pressure drop and multiphase flow. Two correlations were developed in order to determine the mass flow rate of two-phase flow. The first approach is to develop a correlation for K_L and then determine the mass flow rate from it. The other approach is to develop a polynomial fit to determine two-phase mass flow rate. The development and results of these approaches are discussed and compared in the following sections.

4.4 K_L approach

4.4.1 Correlation for mass flow rate

Traditional K_L correlations typically include the density ratio of gases and liquids and the void fraction. A key requirement is that at zero gas fraction, i.e. liquid flow, $K_L = 1$. As a result, $(K_L - 1)/\alpha$ was plotted against different variables such as density ratio, gas fraction and single-phase mass flow rate to test their dependence on $(K_L - 1)/\alpha$. Note that the single-phase mass flow rate $(\dot{m}_{SP})$ used while developing the K_L correlation was different from the mass flow rate of liquid as the pressure drops used in Eqs. 4.11 and 4.12 were that of two-phase flow and not that of liquid phase flow.

$$\dot{m}_{SP,U} = m_U^* \sqrt{2\rho_L \Delta P_{TP,U}} + c_U^* \tag{4.11}$$

$$\dot{m}_{SP,D} = m_D^* \sqrt{2\rho_L \Delta P_{TP,D}} + c_D^* \tag{4.12}$$

4.4.1.1 Effect of single-phase mass flow rate

When paired against the single-phase mass flow rate (Figure 4-8), two trends within the plot can be observed for both upstream and downstream sections. One is a general increase in the value of $(K_L - 1)/\alpha$ with mass flow rate. The other trend is groupings of conditions for which $(K_L - 1)/\alpha$ decreases with increased mass flow rate. At higher flow rates, most of the $(K_L - 1)/\alpha$ values exceeded zero for the upstream section while they remained below zero for the downstream section. This suggests that the values of $K_L > 1$ are related to the flow pattern transitions which occur as bubbly/slug flow from the T junction is initially homogenized in the first elements of the upstream mixer.

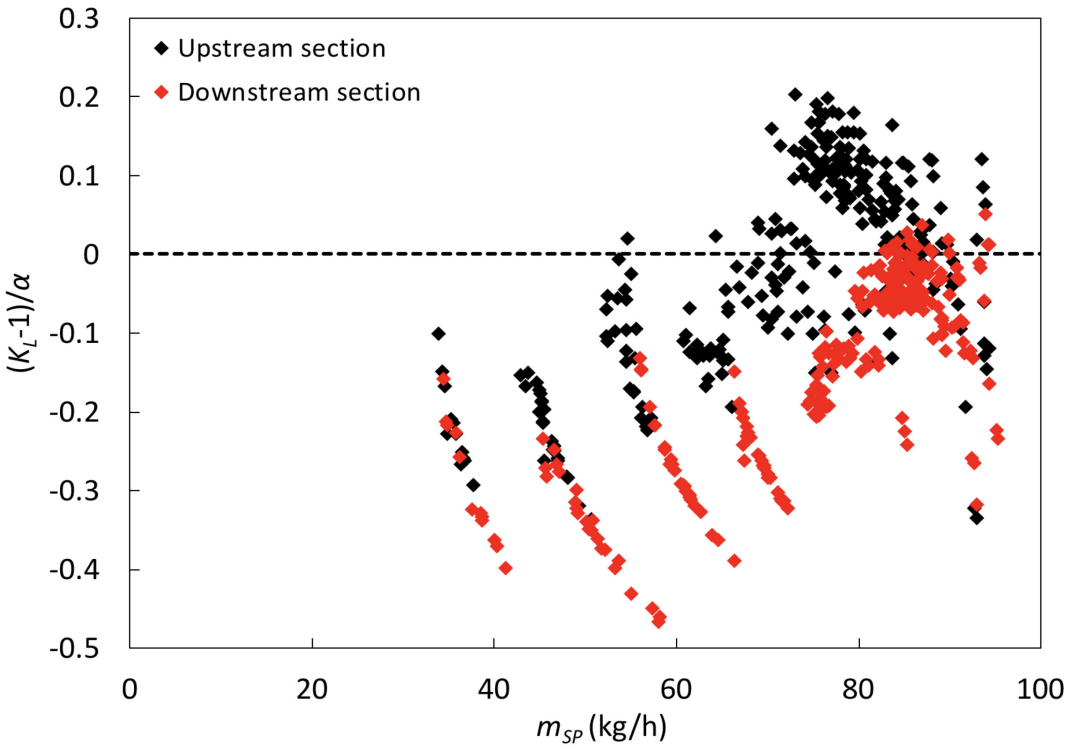

Figure 4-8 *Impact of single-phase mass flow rate on* $\left(K_L-1\right)/\alpha$

4.4.1.2 Effect of gas to liquid density ratio

A clear increasing trend can be observed (Figure 4-9) for the impact of gas to liquid density ratio on $\left(K_L-1\right)/\alpha$. Similar to single-phase mass flow rate, it can be observed that $\left(K_L-1\right)/\alpha$ values went above zero at higher density ratios for upstream section only.

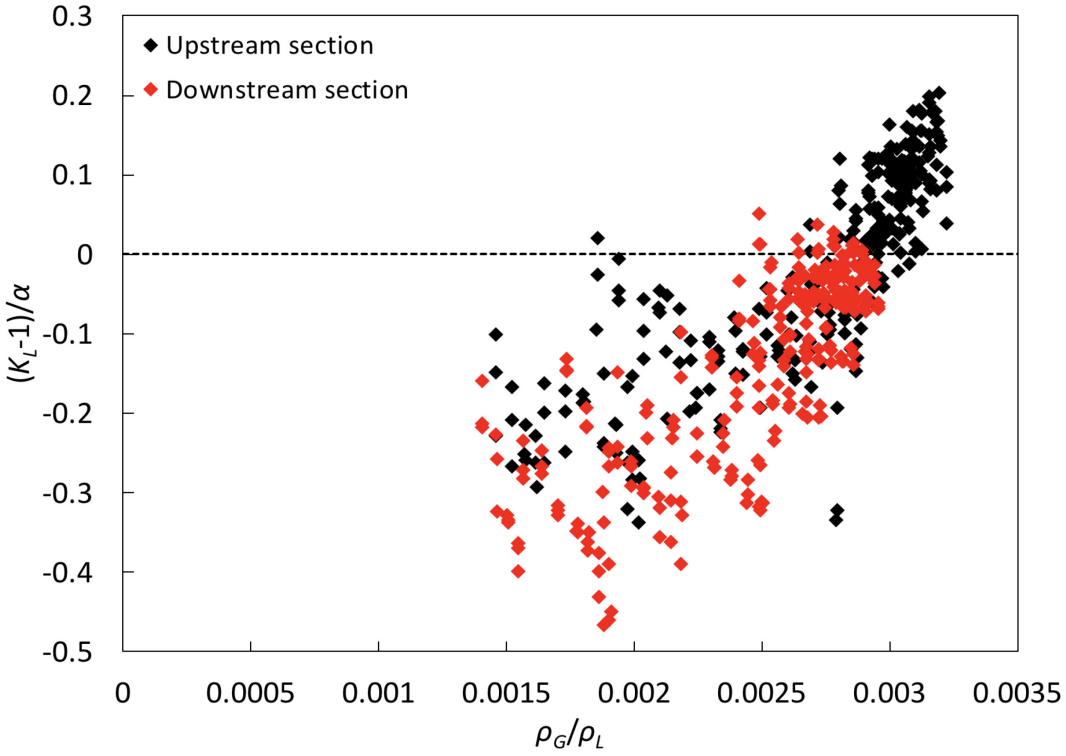

Figure 4-9 *Impact of density ratio on* $(K_L - 1)/\alpha$

4.4.1.3 Effect of gas fraction

The impact of gas fraction on the $(K_L - 1)/\alpha$ parameter is shown in Figure 4-10. It can be observed that the overall trend is decreasing with low gas fractions at the top left and the higher gas fractions at the bottom right. While most of the $(K_L - 1)/\alpha$ values remained less than zero for downstream sections, they went above zero for upstream section, particularly at low and intermediate gas fractions.

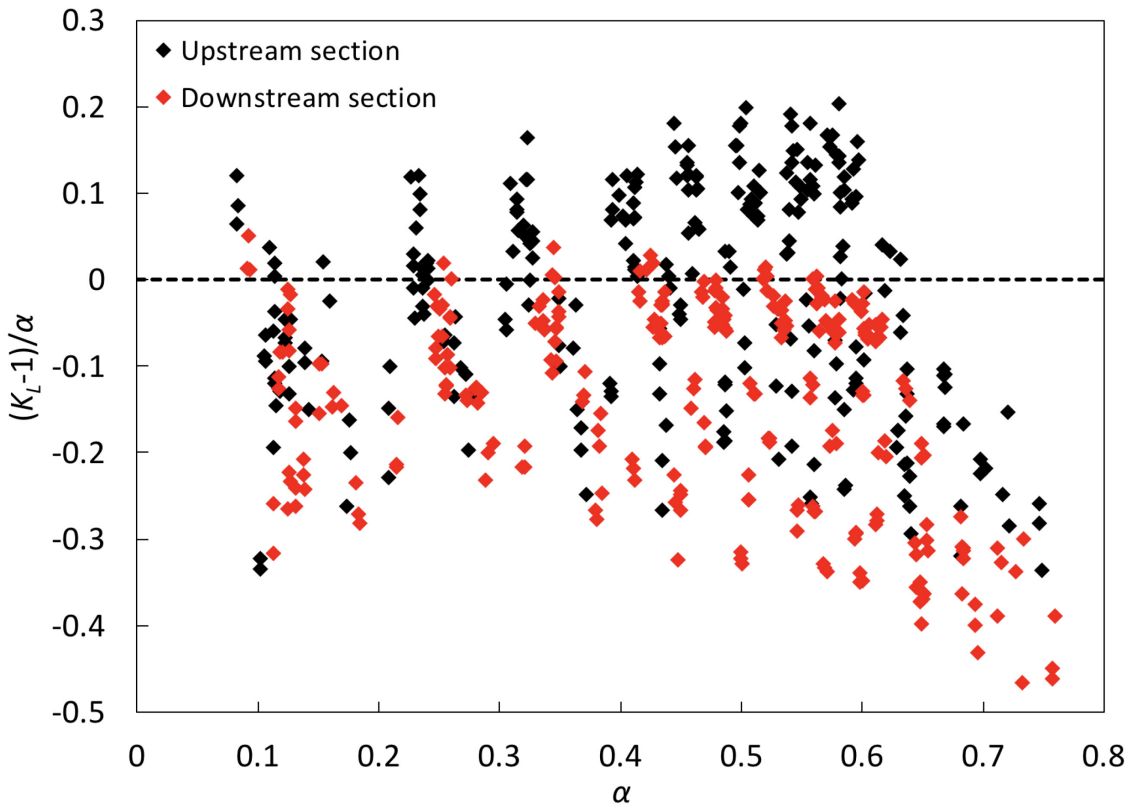

Figure 4-10 *Impact of gas fraction on* $(K_L - 1)/\alpha$

Using the parameters tested and using a linear square fit, correlations were developed to determine $K_{L,U}$ and $K_{L,D}$ as given by Eqs. 4.13 and 4.14. The linear dependence of mass flow rate and density ratio can be observed in the equation as well.

$$K_{L,U} = 1 + \alpha\left(-0.447 - 0.0116\dot{m}_{SP,U} + 521.825\left(\frac{\rho_G}{\rho_L}\right) - 0.655\alpha^2\right) \tag{4.13}$$

$$K_{L,D} = 1 + \alpha\left(-0.585 - 0.00725\dot{m}_{SP,D} + 460.931\left(\frac{\rho_G}{\rho_L}\right) - 0.603\alpha^2\right) \tag{4.14}$$

To observe the dependence of K_L correlation on gas fraction, a plot was drawn between $\left(K_{L,U}-1\right)/\alpha+0.447+0.0116\dot{m}_{SP,U}-521.825\left(\rho_G/\rho_L\right)$ and gas fraction for the upstream section and between $\left(K_{L,D}-1\right)/\alpha+0.585+0.00725\dot{m}_{SP,D}-460.931\left(\rho_G/\rho_L\right)$ and gas fraction for the downstream section as illustrated by Figure 4-11. An overall decreasing trend was observed with increasing gas fraction for both the sections. Also, more spread can be observed in $\left(K_{L,U}-1\right)/\alpha+0.447+0.0116\dot{m}_{SP,U}-521.825\left(\rho_G/\rho_L\right)$ and $\left(K_{L,D}-1\right)/\alpha+0.585+0.00725\dot{m}_{SP,D}-460.931\left(\rho_G/\rho_L\right)$ values at the lower gas fractions compared to intermediate and higher gas fractions. This could be because of the non-homogeneous flow patterns at lower gas flow rates.

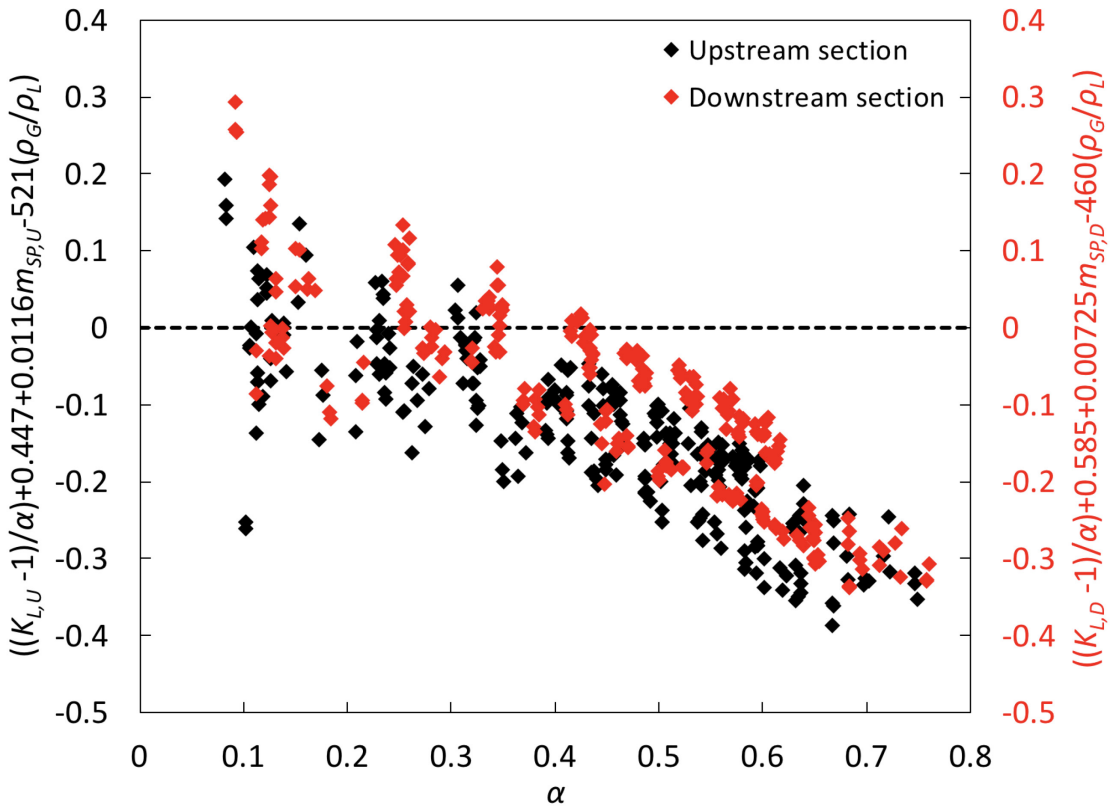

Figure 4-11 *Impact of gas fraction on mass flow and density-corrected K_L values in the upstream (black) and downstream sections (red)*

Mass flow was determined using the K_L correlations developed above (Eqs. 4.13 and 4.14) and was compared with actual mass flow rate in Figure 4-12. Similarly, the mass flow rate from upstream and downstream sections are compared with each other in Figure 4-13. It can be noticed that the mass flow rate values between the upstream and downstream sections are close to each other as expected with residual errors lying between ±5 kg/h.

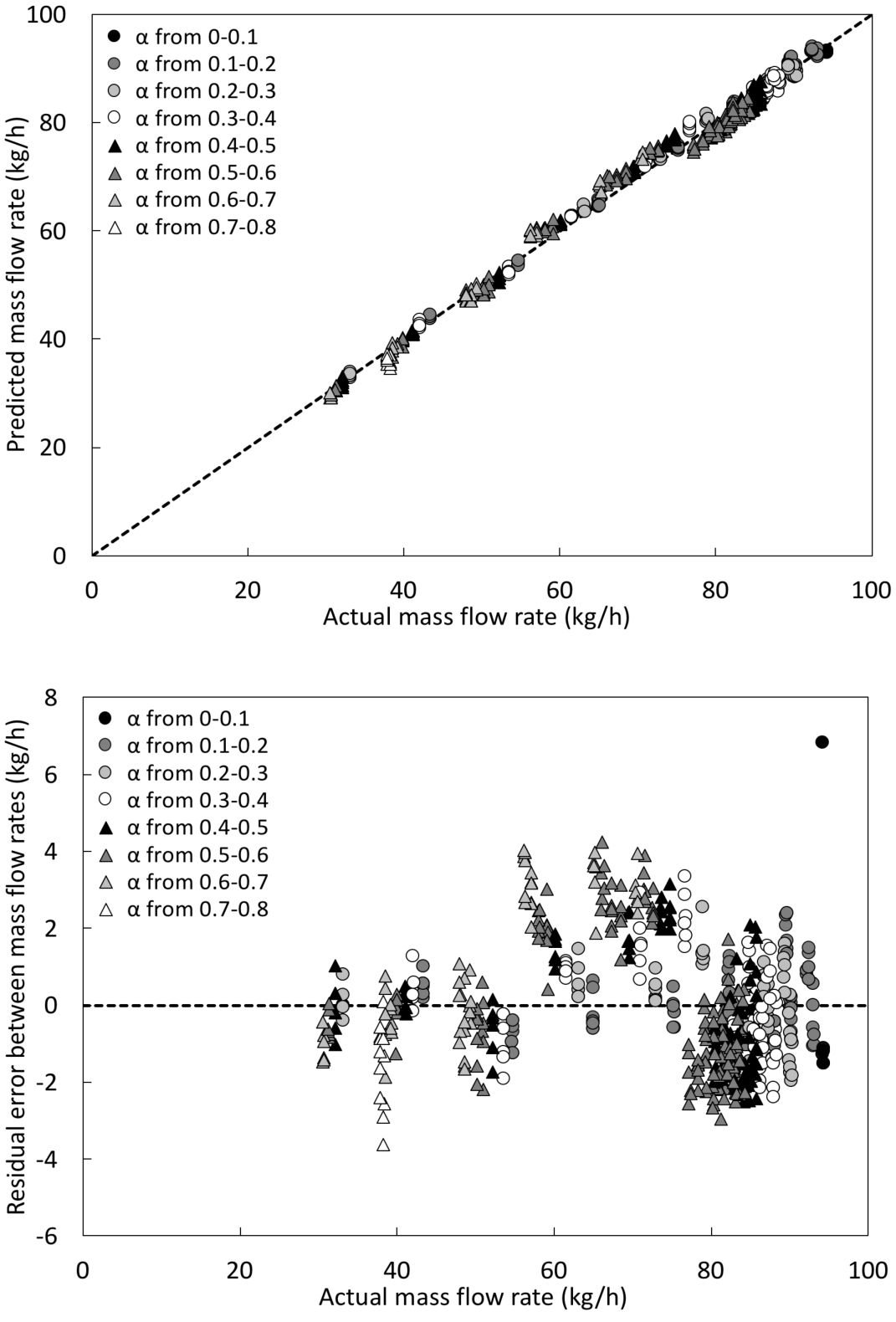

Figure 4-12 *Comparison between mass flow rate predicted using K_L approach and actual mass flow rate (top) and the residual errors between them (bottom)*

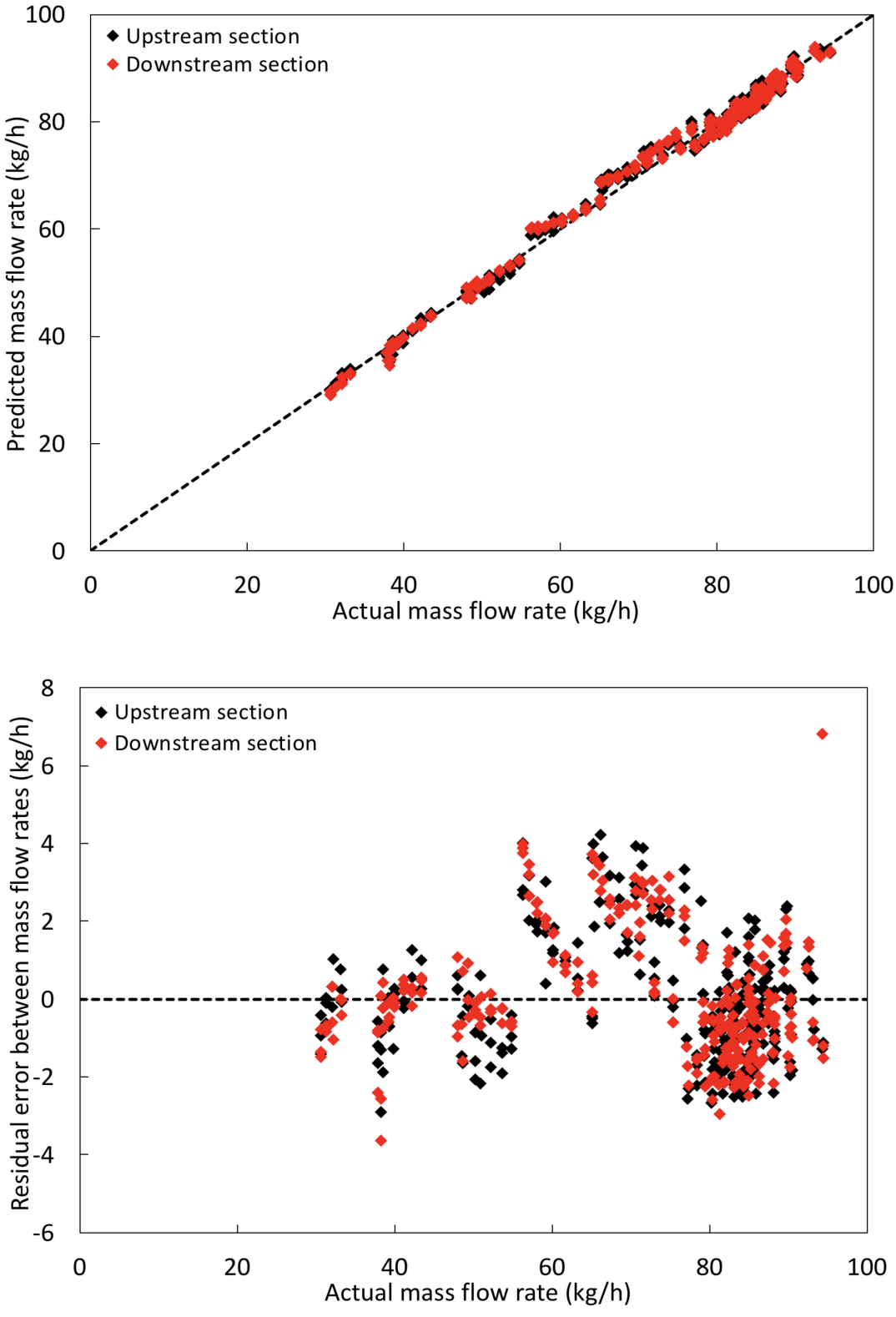

Figure 4-13 *Comparison between mass flow rates predicted for upstream and downstream sections (top) and the residual errors between them (bottom)*

4.4.2 Correlation for gas fraction

Taking the ratio of upstream and downstream mass flow rate equations and applying root-finding approaches to K_L correlations, a value of gas fraction at upstream conditions can be determined such that the following relationship holds true (Eq. 4.15). The relationship between gas fractions at upstream and downstream conditions, which was derived in Appendix A, was also used as given by Eq. 4.17. This approach requires K_L to be sensitive to variations in gas fractions at the mass flow rates and density ratios present.

$$\dot{m}_{TP,U} = \dot{m}_{TP,D} \tag{4.15}$$

$$\frac{\dot{m}_{TP,U}}{\dot{m}_{TP,D}} = \frac{K_{L,U}\left(m_U^* \sqrt{2\rho_L \Delta P_{TP,U}} + c_U^*\right)}{K_{L,D}\left(m_D^* \sqrt{2\rho_L \Delta P_{TP,D}} + c_D^*\right)} \tag{4.16}$$

$$\alpha_D = \frac{1}{1 + \left(\frac{\rho_{G,D}}{\rho_{G,U}}\right)\left(\frac{1-\alpha_U}{\alpha_U}\right)} \tag{4.17}$$

It can be observed from Figure 4-14 that the predicted gas fraction values have a variation of 20 to 40% in the residual errors. It should also be noted that some of the predicted gas fraction values are negative which is not physically possible.

In order to better estimate gas fraction and mass flow rate values, a fully empirical model was also explored.

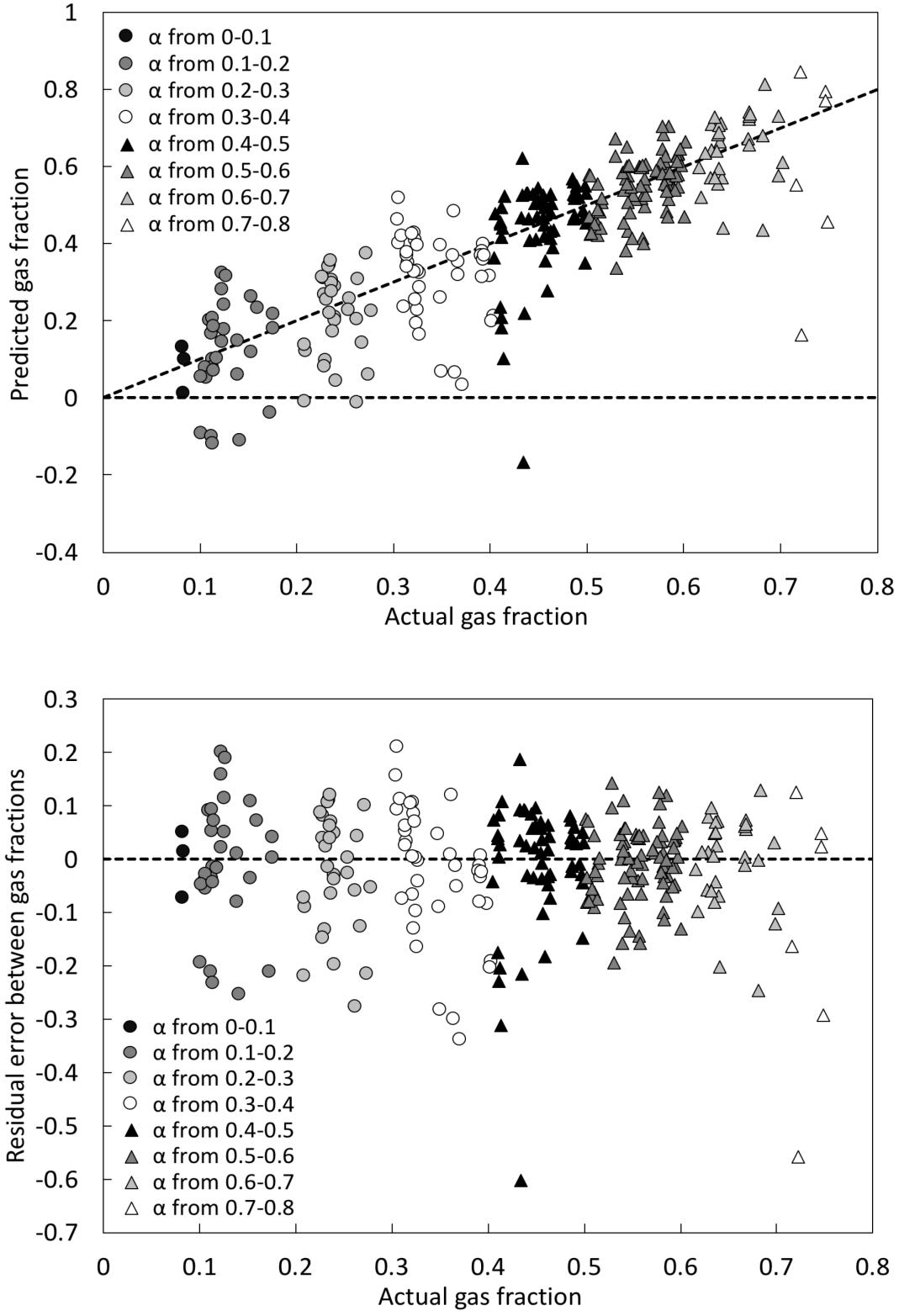

Figure 4-14 *Comparison between gas fraction predicted using K_L approach and actual gas fraction (top) and the residual errors between them (bottom)*

4.5 Fully-empirical approach

4.5.1 Polynomial approach for mass flow rate

Using regression analysis, Eq. 4.18 has been generated to predict the mass flow rate of two-phase flow $\left(\dot{m}_{TP}\right)$ using gas fraction and the ratio of densities of fluids. Note that the gas fraction used in the equation is the actual gas fraction calculated from the individual liquid and gas flow rates sent into the system and not the predicted gas fraction.

$$\begin{aligned}\dot{m}_{TP} = {} & 1.458\dot{m}_{SP} - 2.441\times10^{-2}\dot{m}_{SP}^2 + 3.439\times10^{-4}\dot{m}_{SP}^3 - 1.777\times10^{-6}\dot{m}_{SP}^4 \\ & - 0.329\alpha\dot{m}_{SP} - 2.233\dot{m}_{SP}\left(\frac{\rho_G}{\rho_L}\right) + 42365.256\dot{m}_{SP}\left(\frac{\rho_G}{\rho_L}\right)^2\end{aligned} \tag{4.18}$$

From Figures 4-15 and 4-16, it is evident that Eq. 4.18 provides a reliable estimate for two-phase mass flow rate for both upstream and downstream sections. It can be observed that the equation is more reliable at lower mass flow rates compared to higher mass flow rates with residual errors lying between -5 to 7 kg/h with most of the data in between ±5 kg/h.

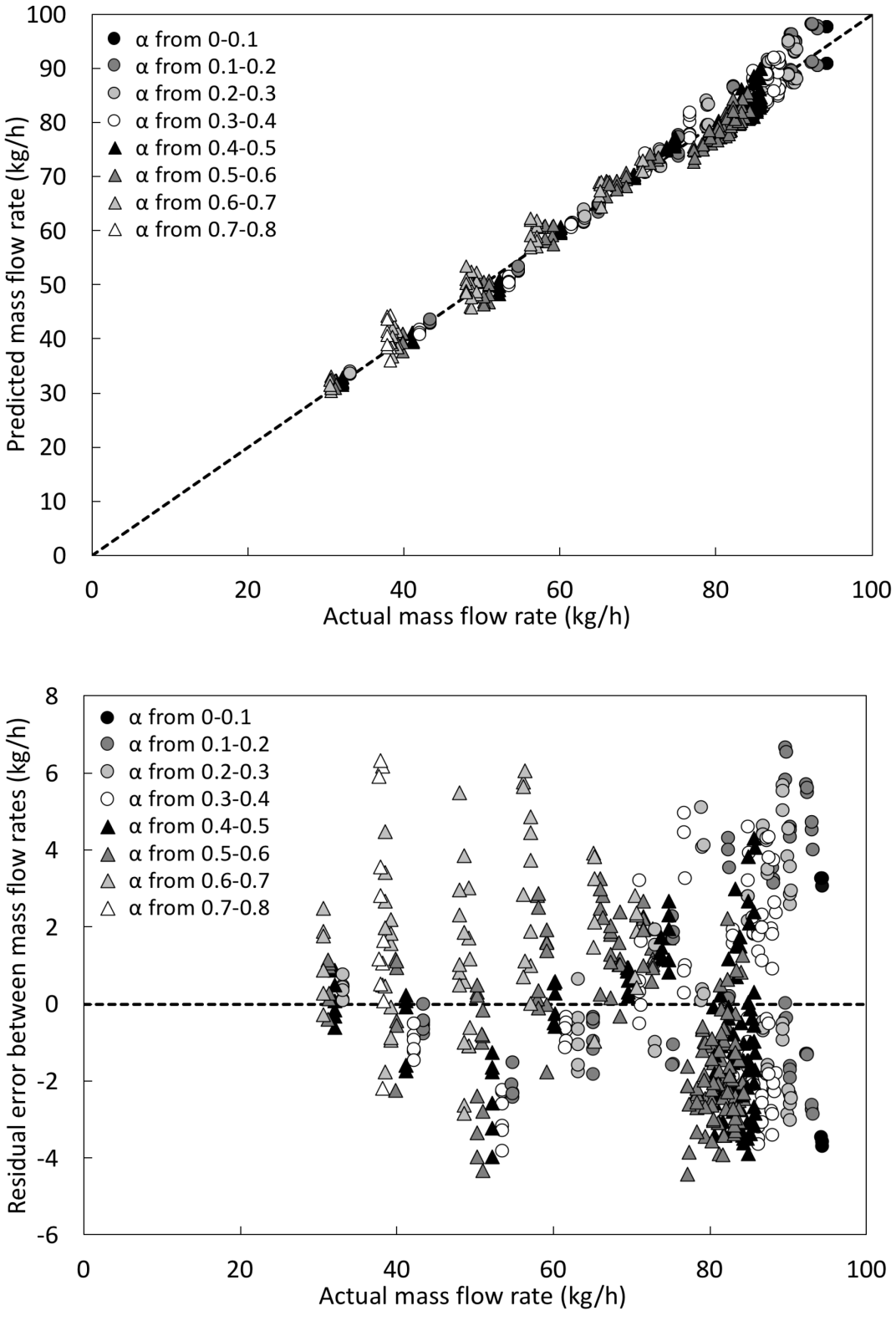

Figure 4-15 *Comparison between predicted and actual mass flow rates using polynomial approach (top) and the residual errors between them (bottom)*

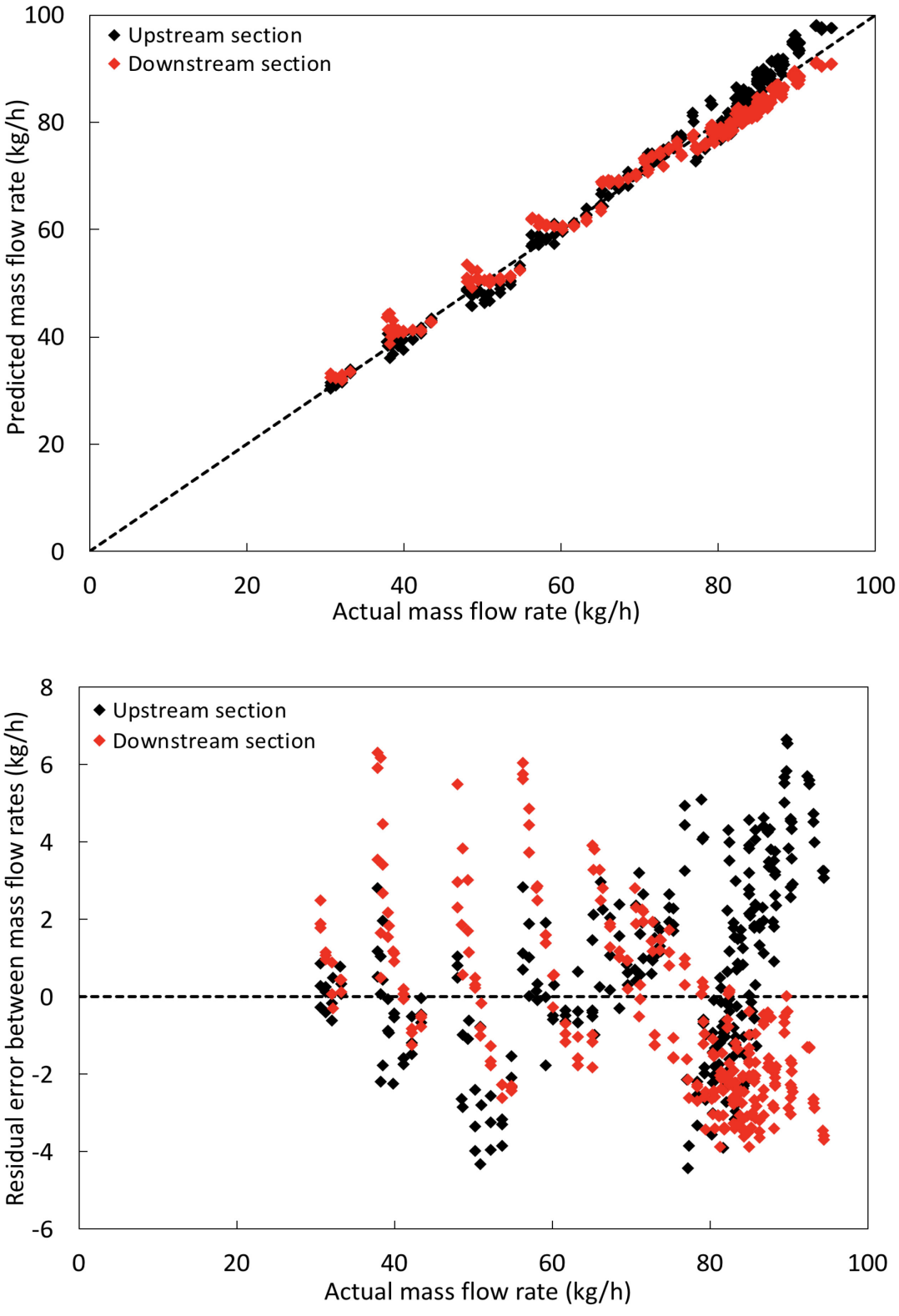

Figure 4-16 *Comparison between mass flow rates predicted for upstream and downstream sections (top) and the residual errors between them (bottom)*

4.5.2 Polynomial approach for gas fraction

A correlation (Eq. 4.19) was developed using regression analysis to determine the gas fraction for two-phase flow using the absolute pressure at P_2, differential pressures across the upstream and downstream sections and the densities of fluids. The predicted gas fraction values determined from this equation were then compared to the known gas fraction values as shown in Figure 4-17.

$$\alpha = -0.313 + 1.948\times10^{-5} P_2 - 4.182\times10^{-11} P_2^2 + 1.065\times10^{-4}\Delta P_U - 3.322\times10^{-4}\Delta P_D + 5.967\times10^{-9}\Delta P_D^2 - 1.229\left(\frac{\Delta P_U}{\Delta P_D}\right) - 0.561\left(\frac{\Delta P_U}{\Delta P_D}\right)^2 + 2.162\left(\frac{\rho_{G,U}}{\rho_{G,D}}\right) \quad (4.19)$$

From the Figure 4-17, it can be observed that the equation generated using regression analysis is giving an estimate of gas fraction for two-phase flow with more than 90% of the residual errors lying in between ±0.1. No negative gas fraction values were observed.

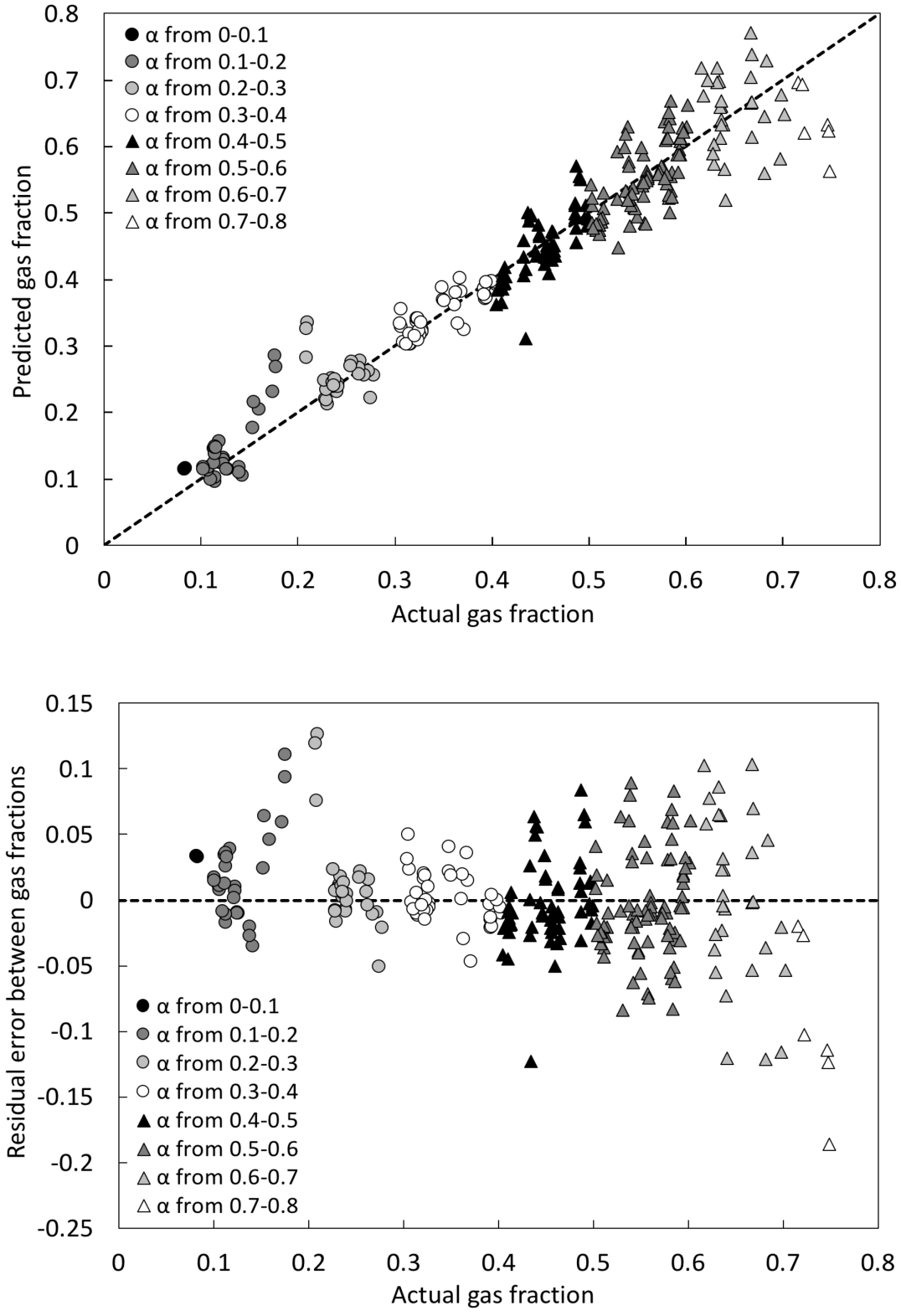

Figure 4-17 *Comparison between predicted gas fraction and actual gas fraction (top) and the residual errors between them (bottom)*

4.6 Comparison between the two approaches

The residual errors for mass flow rate and gas fractions obtained from both K_L and polynomial approaches are compared with each other in Figure 4-18. It can be observed that the K_L correlation gives a better estimate for mass flow rate compared to the polynomial approach with residual errors lying in between ±5 kg/h while the residual errors for polynomial approach are between -5 to 7 kg/h. However, for gas fractions the polynomial approach gives a better estimate than the K_L approach with residual errors lying in between ±0.1 for polynomial approach and ±0.3 for K_L correlation.

As a result, the polynomial correlation was used to predict the gas fraction and subsequently, the K_L correlation was used to estimate the mass flow rate for the DPDE device.

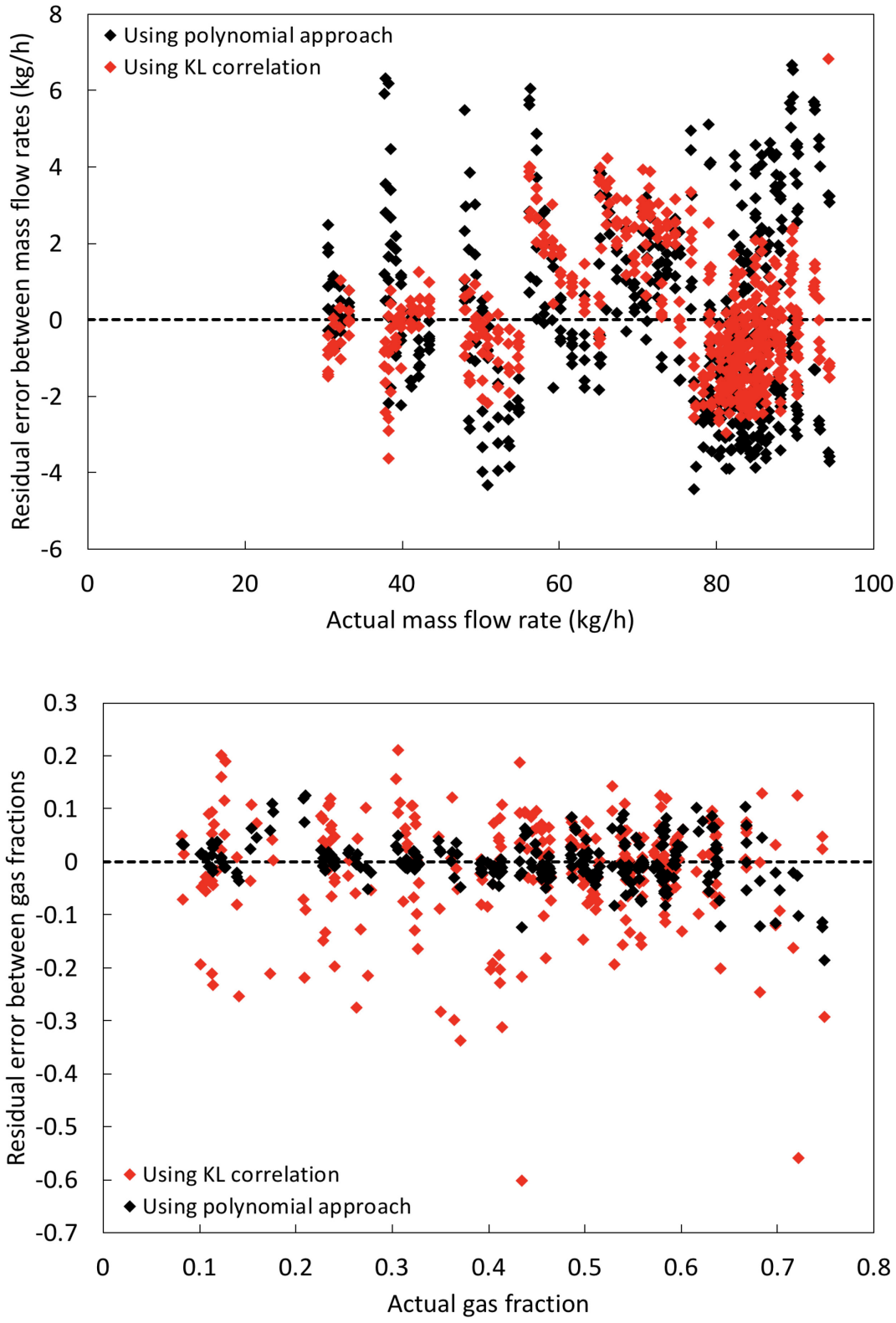

Figure 4-18 *Residual errors between mass flow rates (top) and gas fractions (bottom) from both the approaches*

4.7 DPDE device performance

For the results presented from this point onward (sections 4.7 and 4.8), the predicted gas fractions obtained from the fully-empirical approach were used to calculate the mass flow rate. The correlations developed provide an estimate for mass flow rate with most of the residual errors lying between ±5 kg/h (Figure 4-19).

The density of two-phase flow was also estimated using predicted gas fraction as given by Eq. 4.20.

$$\rho_{TP} = \alpha\rho_G + (1-\alpha)\rho_L \tag{4.20}$$

The residual errors of the densities ranged from ±150 kg/m^3, with most of the data lying between ±100 kg/m^3 (Figure 4-20).

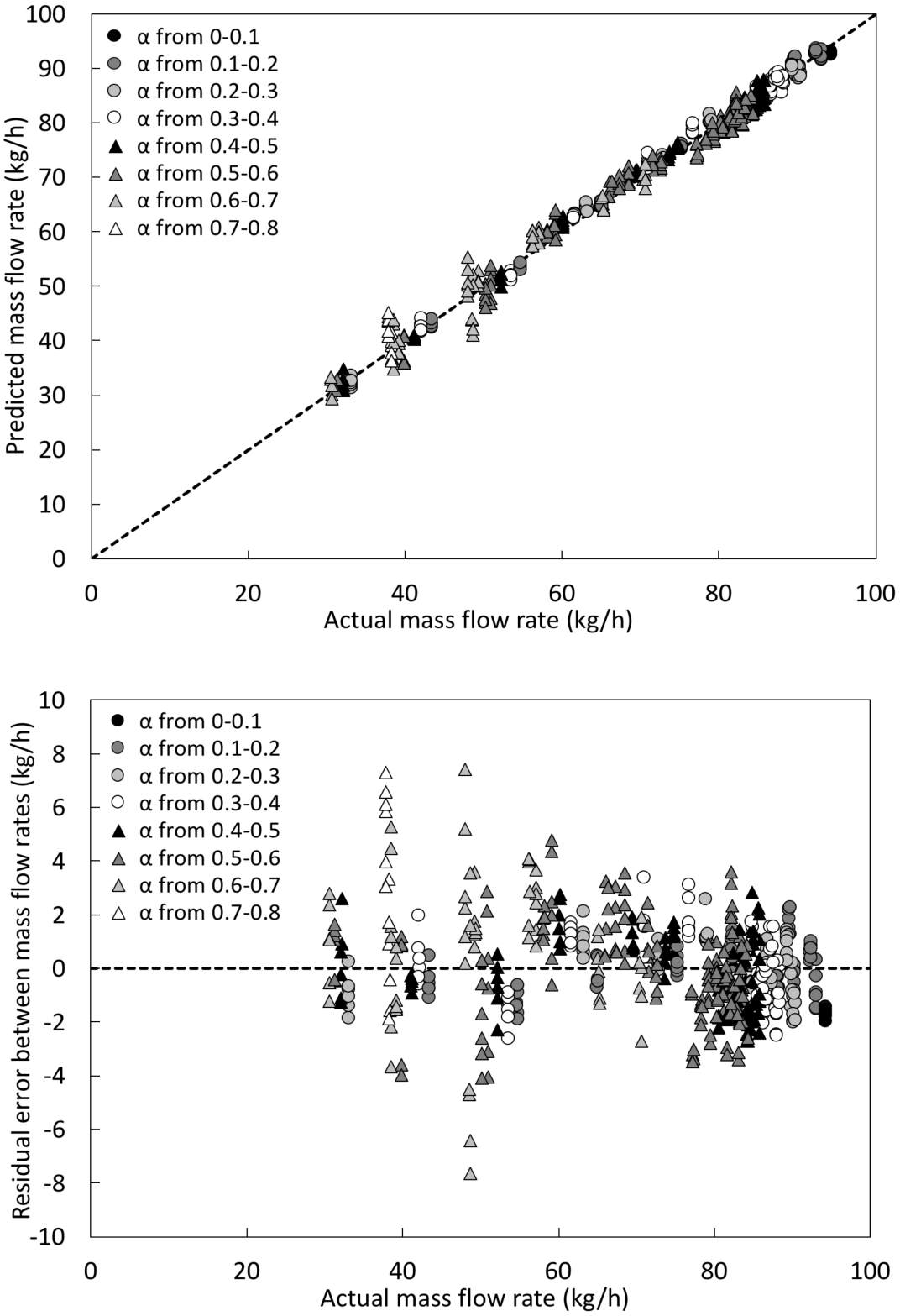

Figure 4-19 *Comparison between fully-predicted and actual mass flow rates (top) and the residual errors between them (bottom)*

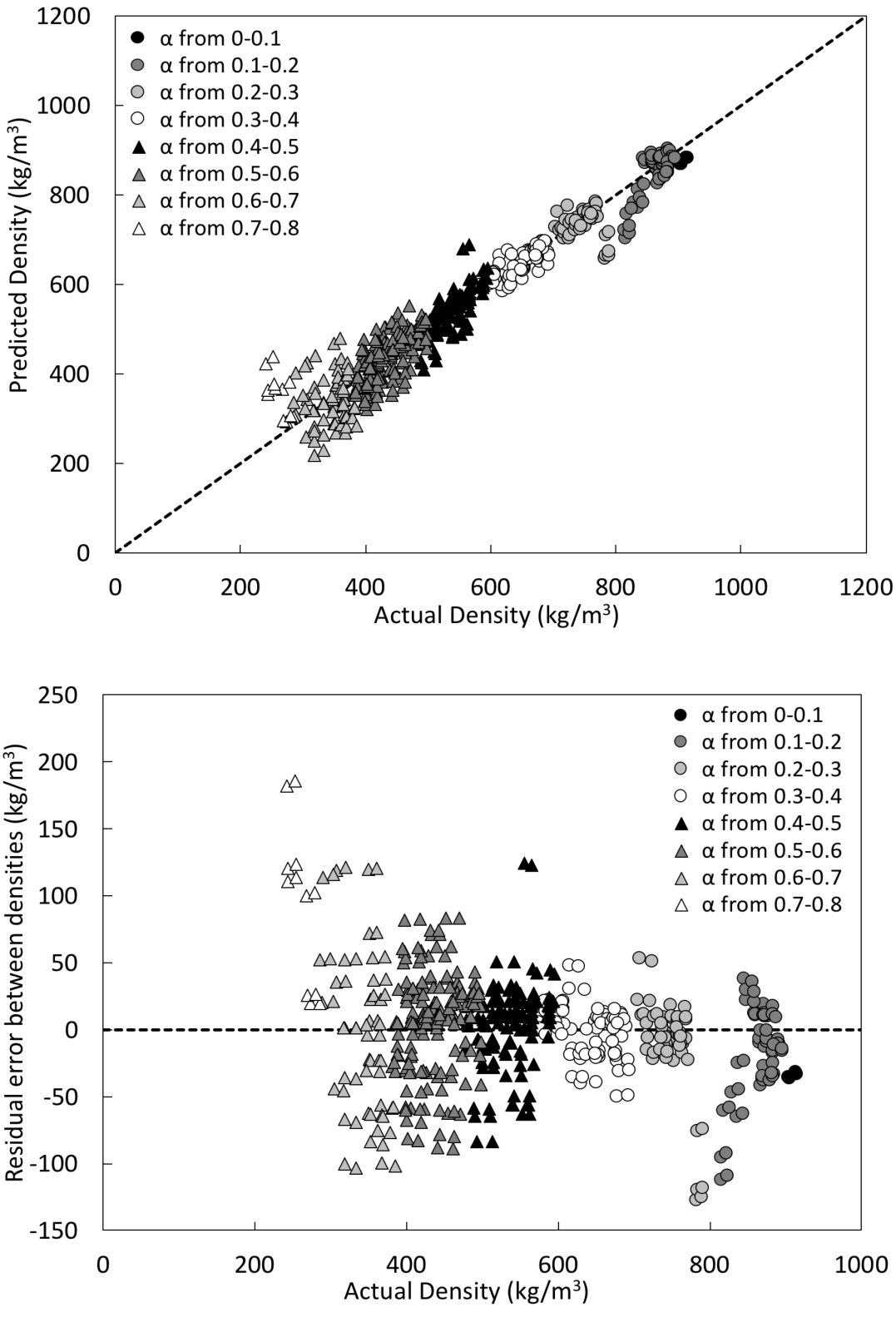

Figure 4-20 *Comparison between fully-predicted density and actual density (top) and the residual errors between them (bottom)*

4.8 Coriolis meter vs DPDE device

The results obtained from the DPDE device were compared with those of Coriolis meter. It can be observed from Figure 4-21 that the mass flow rate obtained from the DPDE device was giving a comparable estimate to that of Coriolis meter. Liu et al. (2001) observed that the mass flow rate errors for raw Coriolis data without any corrections were 20% of the actual values. Similar results were also found here. However, by developing appropriate correlations, the mass flow rate errors obtained from Coriolis meter can be significantly reduced. Henry et al. (2006) have attempted to do this and were able to reduce the error to ±5%. As for density, it can be interpreted that while the error spread was similar for both the devices, the density from the Coriolis meter consistently underestimated the density of two-phase flow. From a density perspective, the DPDE device performed comparably well.

In order to increase the accuracy of the DPDE device, a larger variation in K_L values needs to be created. This can be achieved by increasing the pressure drop between the upstream and downstream sections. The gate valve used for the experiments resulted in a pressure drop of ~2 psi, or approximately 10% of the total absolute pressure of the system. Increasing this pressure drop would result in a greater variation of gas density and gas fraction. This variation would contribute to a larger difference in K_L values between the upstream and downstream pressure drop elements, making the measurement more sensitive to gas fraction.

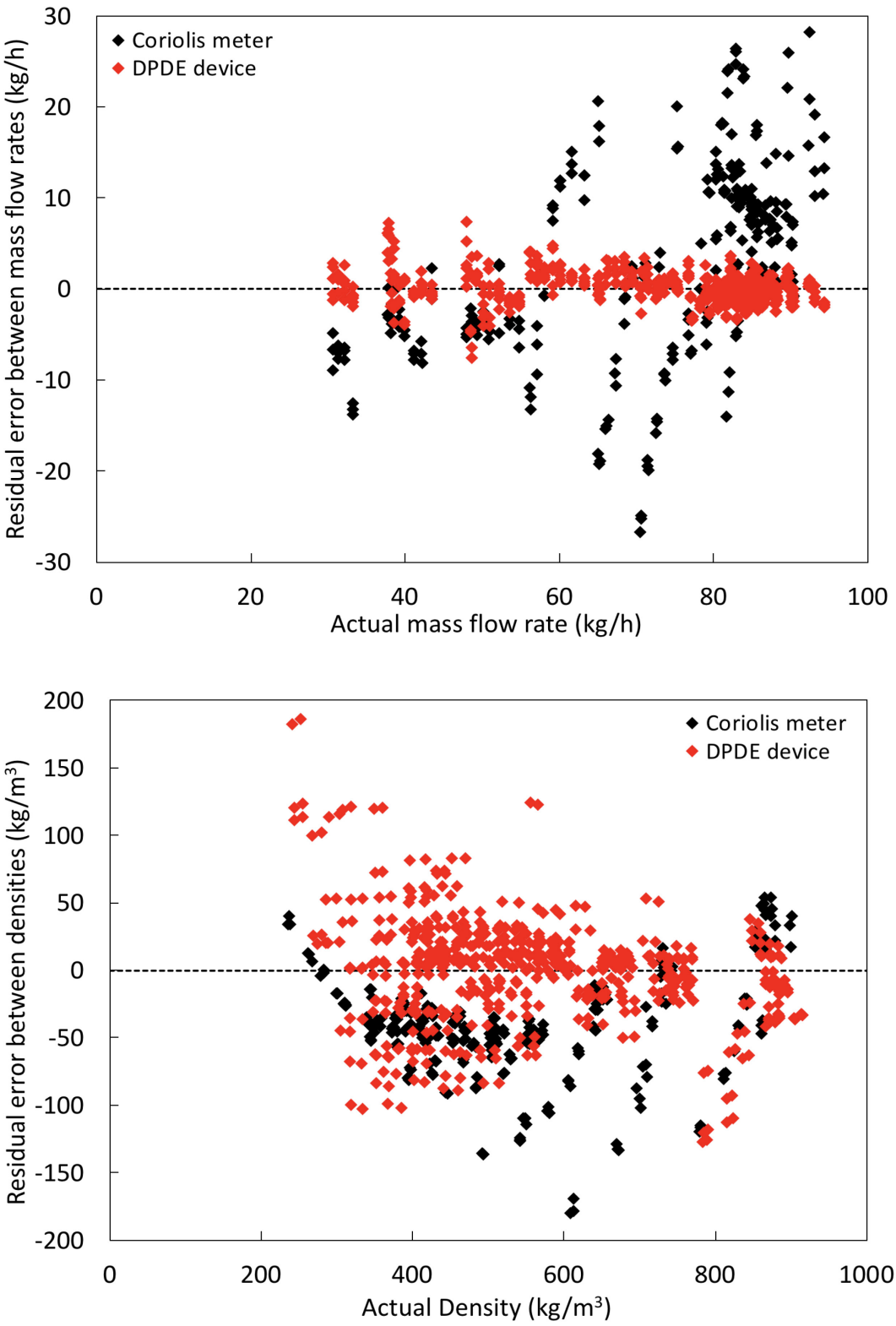

Figure 4-21 *Residual errors between mass flow rates (top) and densities (bottom) obtained from DPDE device and Coriolis meter*

Chapter 5 CONCLUSION

The selection criteria for a two-phase flow meter usually includes three variables, namely cost of the flowmeter, accuracy of the measurement and intrusiveness of the instrument on the two-phase flow. As this thesis demonstrates, a successful estimation of mass flow rate and density of two-phase flow using the DPDE device was accomplished with results comparable to that of Coriolis meter. With the DPDE device, the mass flow rate ranging from 30-100 kg/h was measured with an error of roughly 5% at full scale while the Coriolis meter for the same range gave an error on the order of ±20% at full scale. For density, the Coriolis meter showed a bias towards the underestimation of density, particularly for intermediate gas fractions with residual errors lying between -150 to 50 kg/m^3 whereas the DPDE device has an error spread that is more distributed at the center with most of the data lying between -100 to 100 kg/m^3.

Advantages of using DPDE device over Coriolis meter are its ease of manufacture and lower cost of operation and maintenance. Limitations of the meter include the recalibration of the device for any other fluids. Since there are no dimensionless numbers in the derived relations to account for the properties of other fluids, the equations derived are limited to air-ethanol-water mixture only.

Future work which could aid in the improvement of this metering device includes:

- A standardized pressure drop device such as a Venturi nozzle or an orifice plate can be used in the place of static mixers and its effects on flow patterns and K_L values can be studied.

- As mentioned earlier in the document, the density estimate could be improved by increasing the pressure drop between the upstream and downstream elements. This hypothesis can be experimentally verified by replacing the gate valve between the sections with another one with a smaller flow coefficient value.

- The DPDE device developed can be tested with different fluid pairs and their effects on different parameters can be explored, specifically looking at the impact of fluid properties on the K_L correction.

- The geometry of the static meters can be altered and its impact on K_L correlation can be investigated.

References

Åbro, E., Johansen, G., 1999. Improved void fraction determination by means of multibeam gamma-ray attenuation measurements. Flow Measurement and Instrumentation 10, 99-108.

Åbro, E., Khoryakov, V., Johansen, G., Kocbach, L., 1999. Determination of void fraction and flow regime using a neural network trained on simulated data based on gamma-ray densitometry. Measurement Science and Technology 10, 619.

Anklin, M., Drahm, W., Rieder, A., 2006. Coriolis mass flowmeters: Overview of the current state of the art and latest research. Flow Measurement and Instrumentation 17, 317-323.

Baker, R.C., 2005. Flow measurement handbook: industrial designs, operating principles, performance, and applications. Cambridge University Press.

Barnea, D., 1987. A unified model for predicting flow-pattern transitions for the whole range of pipe inclinations. International Journal of Multiphase Flow 13, 1-12.

Barnea, D., Shoham, O., Taitel, Y., 1982. Flow pattern transition for downward inclined two phase flow; horizontal to vertical. Chemical Engineering Science 37, 735-740.

Beg, N., Toral, H., 1993. Off-site calibration of a two-phase pattern recognition flowmeter. International Journal of Multiphase Flow 19, 999-1012.

Bertani, C., De Salve, M., Malandrone, M., 2010. State-of-Art and selection of techniques in multiphase flow measurement.

Bilgic, A.M., Kunze, J.W., Stegemann, V., Hogendoorn, J., Cerioni, L., Zoeteweij, M., 2015. Multiphase flow metering with nuclear magnetic resonance. tm-Technisches Messen 82, 539-548.

Bø, Ø.L., Nyfors, E., Løland, T., Couput, J.P., 2002. New compact wet gas meter based on a microwave water detection technique and differential pressure flow measurement, 20 th North Sea Flow Measurement Workshop.

Ceccio, S., George, D., 1996. A review of electrical impedance techniques for the measurement of multiphase flows. Journal of Fluids Engineering 118, 391-399.

Chisholm, D., 1967. A theoretical basis for the Lockhart-Martinelli correlation for two-phase flow. International Journal of Heat and Mass Transfer 10, 1767-1778.

Chisholm, D., 1977. Two phase flow through sharp-edged orifices. J. Mech. Eng. Sci 19, 127-129.

Collins, D., Gacesa, M., 1971. Measurement of steam quality in two-phase upflow with venturimeters and orifice plates. Journal of Basic Engineering 93, 11-20.

Corneliussen, S., Couput, J.-P., Dahl, E., Dykesteen, E., Frøysa, K.-E., Malde, E., Moestue, H., Moksnes, P.O., Scheers, L., Tunheim, H., 2005. Handbook of multiphase flow metering. Norwegian Society for Oil and Gas Measurement (NFOGM), Revision 2.

De Leeuw, R., 1997. Liquid correction of Venturi meter readings in wet gas flow, North Sea Flow Measurement Workshop.

De Nevers, N., 2011. Fluid mechanics for chemical engineers. Tata McGraw-Hill.

dos Reis, E., Goldstein Jr, L., 2008. On the measurement of the mass flow rate of horizontal two-phase flows in the proximity of the transition lines which separates two different flow patterns. Flow Measurement and Instrumentation 19, 269-282.

Dualstream, I., 2001. Development of a new intelligent wet gas meter. Solartron ISA, ISA102.

Falcone, G., Hewitt, G., Alimonti, C., 2009. Multiphase flow metering: principles and applications. Elsevier.

Falcone, G., Hewitt, G.F., Alimonti, C., Harrison, B., 2002. Multiphase flow metering: Current trends and future developments. Journal of Petroleum Technology 54, 77-84.

Fincke, J.R., Ronnenkamp, C., Kruse, D., Krogue, J., Householder, D., 1999. Performance characteristics of an extended throat flow nozzle for the measurement of high void fraction multi-phase flows. Idaho National Engineering and Environmental Laboratory, Idaho Falls, ID (US).

G.H. Roshani, E.N., S.A.H. Feghhi, S. Setayeshi, 2015. Flow regime identification and void fraction prediction in two-phase flows based on gamma ray attenuation. Measurement 62 (2015) 25–32, 25-32.

Gysling, D.L., 2007. An aeroelastic model of Coriolis mass and density meters operating on aerated mixtures. Flow Measurement and Instrumentation 18, 69-77.

Gysling, D.L., Loose, D., Morlino, N., 2007. Wet gas metering using sonar-based flow meters and piping pressure loss gradients, Proceedings of the 2007 North Sea Flow Measurement Workshop.

He, D., Lu, B., Li, X., Zhou, R., Bai, B., 2013. A new method to meter wetgas flow based on double differential pressure. Journal of Engineering Thermo physics (China) 34, 878-882.

Henry, M., 2008. Oil and Gas Applications for Digital Coriolis Mass Flow Metering—Introduction. Measurement and Control 41, 203-204.

Henry, M., Tombs, M., Duta, M., Zhou, F.B., Mercado, R., Kenyery, F., Shen, J., Morles, M., Garcia, C., Langansan, R., 2006. Two-phase flow metering of heavy oil using a Coriolis mass flow meter: A case study. Flow Measurement and Instrumentation 17, 399-413.

Henry, M., Tombs, M., Zamora, M., Zhou, F.B., 2013. Coriolis mass flow metering for three-phase flow: A case study. Flow Measurement and Instrumentation 30, 112-122.

Hewitt, G., 2013. Annular two-phase flow. Elsevier.

Hewitt, G.F., Wallis, G.B., 1963. Flooding and associated phenomena in falling film flow in a tube. United Kingdom Atomic Energy Authority. Research Group. Atomic Energy Research Establishment, Harwell Berks, England.

Hong-jian, Z., Wei-ting, Y., Zhi-yao, H., 2005. Investigation of oil-air two-phase mass flow rate measurement using Venturi and void fraction sensor. Journal of Zhejiang University-SCIENCE A 6, 601-606.

Hua, C., Geng, Y., 2012. Wet gas meter based on the vortex precession frequency and differential pressure combination of swirlmeter. Measurement 45, 763-768.

Hua, C., Geng, Y., 2013. Wet gas metering technique based on slotted orifice and swirlmeter in series. Flow Measurement and Instrumentation 30, 138-143.

Huang, Z., Li, X., Li, H., 2007. Liquid-liquid two-phase flow measurement based on Venturi meter and turbine flowmeter. JOURNAL OF ENGINEERING THERMOPHYSICS 28, 808.

Huang, Z., Wang, B., Li, H., 2003. Application of electrical capacitance tomography to the void fraction measurement of two-phase flow. IEEE Transactions on Instrumentation and Measurement 52, 7-12.

Huang, Z., Xie, D., Zhang, H., Li, H., 2005. Gas–oil two-phase flow measurement using an electrical capacitance tomography system and a Venturi meter. Flow Measurement and Instrumentation 16, 177-182.

James, R., 1965. Metering of steam-water two-phase flow by sharp-edged orifices. Proceedings of the Institution of Mechanical Engineers 180, 549-572.

Li, Y., Wang, J., Geng, Y., 2009. Study on wet gas online flow rate measurement based on dual slotted orifice plate. Flow Measurement and Instrumentation 20, 168-173.

Lide, F., Tao, Z., Ningde, J., 2007. A comparison of correlations used for Venturi wet gas metering in oil and gas industry. Journal of Petroleum Science and Engineering 57, 247-256.

Lindken, R., Merzkirch, W., 2002. A novel PIV technique for measurements in multiphase flows and its application to two-phase bubbly flows. Experiments in fluids 33, 814-825.

Liu, R., Fuent, M., Henry, M., Duta, M., 2001. A neural network to correct mass flow errors caused by two-phase flow in a digital coriolis mass flowmeter. Flow Measurement and Instrumentation 12, 53-63.

McKnight, C.A., Hackman, L.P., Grace, J.R., Macchi, A., Kiel, D., Tyler, J., 2008. Fluid Dynamic Studies in Support of an Industrial Three-Phase Fluidized Bed Hydroprocessor. The Canadian Journal of Chemical Engineering 81, 338-350.

Meng, Z., Huang, Z., Wang, B., Ji, H., Li, H., Yan, Y., 2010. Air–water two-phase flow measurement using a Venturi meter and an electrical resistance tomography sensor. Flow Measurement and Instrumentation 21, 268-276.

Meribout, M., Al-Rawahi, N.Z., Al-Naamany, A.M., Al-Bimani, A., Al-Busaidi, K., Meribout, A., 2010. A multisensor intelligent device for real-time multiphase flow metering in oil fields. IEEE Transactions on Instrumentation and Measurement 59, 1507-1519.

Morris, S., 1985. Two phase pressure drop across valves and orifice plates, Proceedings of the European Two Phase Flow Group Meeting, Marchwood Engineering Laboratories, Southampton, UK.

O'Banion, T., 2013. Coriolis: The Direct Approach to Mass Flow Measurement. Chemical Engineering Progress 109, 41-46.

Oliveira, J.L.G., Passos, J.C., Verschaeren, R., van der Geld, C., 2009. Mass flow rate measurements in gas–liquid flows by means of a venturi or orifice plate coupled to a void fraction sensor. Experimental Thermal and Fluid Science 33, 253-260.

Paranjape, S., Ritchey, S.N., Garimella, S.V., 2012. Electrical impedance-based void fraction measurement and flow regime identification in microchannel flows under adiabatic conditions. International Journal of Multiphase Flow 42, 175-183.

Rajan, V., Ridley, R., Rafa, K., 1993. Multiphase flow measurement techniques--A review. Journal of Energy Resources Technology;(United States) 115.

Reader-Harris, M., 2016. Orifice plates and venturi tubes. Springer.

Reizner, J., 2003. Coriolis-the almost perfect flowmeter. Computing and Control Engineering 14, 28-33.

Roshani, G., Nazemi, E., Feghhi, S., Setayeshi, S., 2015. Flow regime identification and void fraction prediction in two-phase flows based on gamma ray attenuation. Measurement 62, 25-32.

Roul, M.K., Dash, S.K., 2012. Single-phase and two-phase flow through thin and thick orifices in horizontal pipes. Journal of Fluids Engineering 134, 091301.

Saadawi, A., Grattan, E., Dempster, W., 1999. Two phase pressure loss in orifice plates and gate valves in large diameter pipes, Proceedings of the 2nd Symposium on Two-Phase Flow Modelling and Experimentation, GP Celata, PD Marco, RK Shah, eds., ETS, Pisa, Italy.

Simpson, H., Rooney, D., Grattan, E., 1983. Two phase flow through gate valves and orifice plates, International conference on the physical modelling of multi-phase flow, pp. 25-40.

Smith, R., Leang, J., 1975. Evaluations of correlations for two-phase flowmeters three current–one new. Journal of Engineering for Power 97, 589-593.

Steven, R.N., 2002. Wet gas metering with a horizontally mounted Venturi meter. Flow Measurement and Instrumentation 12, 361-372.

Stewart, D.G., Brown, G., Hodges, D., 2002. Wet gas Venturi metering, SPE Annual Technical Conference and Exhibition. Society of Petroleum Engineers.

Sun, Z., 2010. Mass flow measurement of gas–liquid bubble flow with the combined use of a Venturi tube and a vortex flowmeter. Measurement Science and Technology 21, 055403.

Taitel, Y., Bornea, D., Dukler, A., 1980. Modelling flow pattern transitions for steady upward gas-liquid flow in vertical tubes. AIChE Journal 26, 345 -354.

Tjugum, S., Hjertaker, B., Johansen, G., 2002. Multiphase flow regime identification by multibeam gamma-ray densitometry. Measurement Science and Technology 13, 1319.

Triplett, K., Ghiaasiaan, S., Abdel-Khalik, S., LeMouel, A., McCord, B., 1999. Gas–liquid two-phase flow in microchannels. International Journal of Multiphase Flow 25, 395-410.

Wallis, G., 1962. General correlations for the rise velocity of cylindrical bubbles in vertical tubes. General Electric Co. General Engineering Lab., Schenectady, NY.

Wang, D., 2012. Gas-Liquid Two-Phase Flow Rate Measurements by Flow Division and Separation Method, Flow Measurement. InTech.

Wang, T., Baker, R., 2014. Coriolis flowmeters: a review of developments over the past 20 years, and an assessment of the state of the art and likely future directions. Flow Measurement and Instrumentation 40, 99-123.

Watson, G.G., McFarlane, M., Vaughan, V., 1967. Two-phase pressure drop with a sharp-edged orifice. National Engineering Laboratory.

White, F.M., 2003. Fluid mechanics. 5th. Boston: McGraw-Hill Book Company.

Wylie, S., Shaw, A., Al-Shamma'a, A., 2006. RF sensor for multiphase flow measurement through an oil pipeline. Measurement Science and Technology 17, 2141.

Xing, L.C., Geng, Y.F., Hua, C.Q., Zhu, H., Rieder, A., Drahm, W., Bezdek, M., 2014. A combination method for metering gas-liquid two-phase flows of low liquid loading applying ultrasonic and Coriolis flowmeters. Flow Measurement and Instrumentation 37, 135-143.

Xu, L., Xu, J., Dong, F., Zhang, T., 2003. On fluctuation of the dynamic differential pressure signal of Venturi meter for wet gas metering. Flow Measurement and Instrumentation 14, 211-217.

Xu, L., Zhou, W., Li, X., Wang, M., 2011. Wet-gas flow modeling for the straight section of throat-extended venturi meter. IEEE Transactions on Instrumentation and Measurement 60, 2080-2087.

Xu, Y., Yuan, C., Long, Z., Zhang, Q., Li, Z., Zhang, T., 2013. Research the wet gas flow measurement based on dual-throttle device. Flow Measurement and Instrumentation 34, 68-75.

Yanfeng, G., Zheng, J., Tianming, S., Gang, S., 2007. Wet gas meter development based on slotted orifice couple and neural network techniques. Chinese Journal of Chemical Engineering 15, 281-285.

Zeghloul, A., Azzi, A., Saidj, F., Messilem, A., Azzopardi, B.J., 2017. Pressure Drop Through Orifices for Single-and Two-Phase Vertically Upward Flow—Implication for Metering. Journal of Fluids Engineering 139, 031302.

Zhang, F., Dong, F., Tan, C., 2010. High GVF and low pressure gas–liquid two-phase flow measurement based on dual-cone flowmeter. Flow Measurement and Instrumentation 21, 410-417.

Zhang, H.J., Lu, S.J., Yu, G.Z., 1992. An investigation of two-phase flow measurement with orifices for low-quality mixtures. International Journal of Multiphase Flow 18, 149-155.

Appendix A

Relationship between upstream and downstream gas fractions

Gas fraction is defined as the ratio of volumetric flow rates of gas to the total volumetric flow rate of two-phase flow. This is given by Eqs. A.1 and A.2 for upstream and downstream sections respectively.

$$\alpha_U = \frac{\dot{V}_{G,U}}{\dot{V}_{G,U} + \dot{V}_L} \tag{A.1}$$

$$\alpha_D = \frac{\dot{V}_{G,D}}{\dot{V}_{G,D} + \dot{V}_L} \tag{A.2}$$

Eq. A.1 can also be represented as follows.

$$\dot{V}_{G,U} = \left(\dot{V}_{G,U} + \dot{V}_L\right)\alpha_U \tag{A.3}$$

Recognizing that the mass flow rates in the upstream and downstream sections are equal, and from the definition of density, the following relationship can be derived.

$$\dot{V}_{G,D} = \left(\frac{\rho_{G,U}}{\rho_{G,D}}\right)\dot{V}_{G,U} \tag{A.4}$$

Eq. A.5 was obtained by substituting Eq. A.3 and A.4 in Eq. A.2.

$$\alpha_D = \frac{\dot{V}_{G,D}}{\dot{V}_{G,D} + \dot{V}_L} = \frac{\left(\frac{\rho_{G,U}}{\rho_{G,D}}\right)\left(\dot{V}_{G,U} + \dot{V}_L\right)\alpha_U}{\left(\frac{\rho_{G,U}}{\rho_{G,D}}\right)\left(\dot{V}_{G,U} + \dot{V}_L\right)\alpha_U + \dot{V}_L} \tag{A.5}$$

By applying appropriate transformations as shown in Eqs. A.6, A.7 and A.8, the relationship between the upstream and downstream gas fraction can be obtained (Eq. A.9).

$$\alpha_D = \frac{\left(\frac{\rho_{G,U}}{\rho_{G,D}}\right)\left(\frac{\dot{V}_{G,U} + \dot{V}_L}{\dot{V}_L}\right)\alpha_U}{\left(\frac{\rho_{G,U}}{\rho_{G,D}}\right)\left(\frac{\dot{V}_{G,U} + \dot{V}_L}{\dot{V}_L}\right)\alpha_U + 1} \tag{A.6}$$

$$1 - \alpha_U = 1 - \frac{\dot{V}_{G,U}}{\dot{V}_{G,U} + \dot{V}_L} = \frac{\dot{V}_L}{\dot{V}_{G,U} + \dot{V}_L} \tag{A.7}$$

$$\alpha_D = \frac{\left(\frac{\rho_{G,U}}{\rho_{G,D}}\right)\left(\frac{\alpha_U}{1-\alpha_U}\right)}{\left(\frac{\rho_{G,U}}{\rho_{G,D}}\right)\left(\frac{\alpha_U}{1-\alpha_U}\right) + 1} \tag{A.8}$$

$$\alpha_D = \frac{1}{1 + \left(\frac{\rho_{G,D}}{\rho_{G,U}}\right)\left(\frac{1-\alpha_U}{\alpha_U}\right)} \tag{A.9}$$